1 Twirling torticones: hydrostatics and hydrodynamics of helically-coiled ammonoids

2

- 3 David J. Peterman¹, Nicholas Hebdon¹, Ryan C. Shell², Kathleen A. Ritterbush¹
- ¹University of Utah, Salt Lake City, Utah, USA.
- ²Cincinnati Museum Center, Cincinnati, Ohio, USA.
- 6 < David.Peterman@utah.edu>

7

8

9

10

11

12

13

14

15

16

17

18

19

20

21

22

23

24

Abstract

Of the many shell morphologies produced by ammonoid cephalopods, the helical torticone shape appears poorly-suited to rapid locomotion. We investigate torticone hydrostatics and hydrodynamics through virtual modeling, computational fluid dynamics simulations, and water-chamber experiments, using the Cenomanian (Cretaceous) turrilitid Mariella brazoensis (Roemer, 1852) as a test case. Our hydrostatic model suggests that *M. brazoensis*, and other torticones, could attain neutral buoyancy. This morphotype is highly stable compared to planispiral cephalopods with a slightly tilted, apex-upward orientation. The corresponding mass distribution, relative to the source of jet propulsion at the hyponome, suggests that jet thrust would be more efficiently transmitted into upwards movement than horizontal movement. Most directions of thrust would send the shell spinning about its vertical axis. We 3D printed shell models to have either surpluses or deficiencies in buoyancy that imparted estimated thrusts of extant cephalopod analogues in the vertical directions within a water chamber. The models consistently rotate aperture-backwards during upward movement, and aperture-forwards during downward movement. A neutrally buoyant model was used to assess rotational aptitude during active locomotion. The model required low torques to sustain rotation. Simulations of water flow around the shell support the movement directions observed in the physical experiments and demonstrate that hydrodynamic drag is lower in the vertical directions than the horizontal directions. These results show that the animal within a torticone shell could spin about its vertical axis easily; perhaps even

simple respiration could have allowed rotation at ~20 degrees per second. Hydrostatic and hydrodynamic properties of torticones suggest that rotation and vertical movement potential constrained the behavior of these helically-coiled cephalopods. We interpret that torticone ammonoids, prominent throughout neritic and epeiric seas during the Albian and Cenomanian (Cretaceous), may have used passive spiral motions to feed upon small food items through the water column, and may have had low metabolic demands compared to modern-day coleoids.

INTRODUCTION

25

26

27

28

29

30

31

32

33

34

35

36

37

38

39

40

41

42

43

44

45

46

47

48

Torticone cephalopods had external shells that were coiled in a helical fashion. While their shells have invited comparison with gastropods (Berry, 1928; Ebel, 1992; Wiedmann, 1973), they were chambered, and like other ectocochleate (externally shelled) cephalopods, served as buoyancy apparatuses. These helical shells were convergent, appearing in several higher taxa of both nautiloids and ammonoids. Torticonic nautiloids were relatively scarce, but present from the Ordovician to Devonian within Oncocerida, Discocerida, and Barrandeocerida (Teichert et al., 1964; Ward, 1979a). During the Mesozoic, torticonic ammonoids are represented by Cochloceratidae in the Triassic, a spiroceratid in the Jurassic, and many turrilitoids in the Cretaceous (Dietl, 1973; Ward, 1979a; Wright et al., 1996; Monnet et al., 2015). While torticone shells were generally brief experiments among ectocochleate cephalopods, the Turrilitidae flourished, becoming diverse (~170 species; Klinger and Kennedy, 1978; Klinger, 1981), and attaining an almost cosmopolitan distribution during the Late Cretaceous (Kennedy and Cobban, 1976; Wright et al., 1996; Page, 1996; Ifrim et al., 2015). Their wide biogeographic distribution and abundance makes turrilitids very useful as biostratigraphic index fossils (Cobban, 1971; Kennedy and Klinger, 1975; Kennedy and Cobban, 1976; Kennedy et al., 2005). These qualities suggest that they were important components of marine ecosystems during the middle Cretaceous (middle Albian to late Cenomanian). Despite their inferred ecological significance, little is known about the life habit of turrilitids, and other torticones. Based on shell shape, previous authors have suggested torticones were

poor at horizontal movement (Ward, 1979a; Klinger, 1981; Batt, 1989; Westermann, 1996; Naglik et al., 2015a). It is poorly understood how these cephalopods were able to become so successful, especially considering their presumed locomotory limitations.

Here, we examine the anatomical features that constrain torticone motility and the geological context that frames their potential ecology. While the turrilitid *Mariella brazoensis* (Roemer, 1852) is used as a test case in this study, much of this context is applicable to the broader torticone morphotype.

Torticone Morphology and Anatomy

A biologically diverse range of cephalopods evolved disparate shapes of torticone shells, each providing clues to their possible ecological roles through time. While we do not project one life habit to suit all these diverse and disparate animals, we describe below the features that constrain their range of capabilities in life.

Although many different shapes of helical torticone shells existed, it appears that each individual ammonoid maintained a set geometry throughout life (after the embryonic shell; Drushchits et al., 1977). This somewhat isometric shell growth in many torticone ammonoids suggest that their hydrostatic properties were well-constrained and did not change much throughout ontogeny. This contrasts with other heteromorphs, in which it is common for an individual to alter its overall external shell shape throughout growth (i.e., Raup, 1967; Westermann 1996). Between ammonoid species, different torticone shells vary in apical angles (acuteness of spire), ornamentation patterns, siphuncle positions, septal morphology, as well as the presence of hyponomic sinuses or rostra (Ward, 1979a; Klinger, 1981; Wright et al., 1996; Matsumoto and Kawashita, 1999; Matsumoto et al., 1999). These morphological features, most of which are maintained throughout ontogeny, may have had distinct impacts on the animals' maneuverability. Klinger (1981) suggested that morphs with low apical angles would have had lower drag moving through the water in the upward (adapical) direction. The helical shell may have hydrodynamically interacted with water in a corkscrew fashion during vertical movement, which could be triggered by deliberate upward jet propulsion, by buoyancy manipulation, and/or in response to incident fluid catching the shoulders of each whorl. The consistently tilted ornament on

the shells could have also influenced water flow. However, many turrilitids are preserved as steinkerns (Kennedy and Cobban, 1976; Klinger and Kennedy, 1978; Kennedy et al., 2005), which obscures the morphology of their complete ornamentation. Other turrilitoid ammonoids exhibit similar torticone coiling, mostly in their subadult stages (e.g. Nostoceratidae). During these helically-coiled, subadult stages, these heteromorphs may have shared similar hydrostatic and hydrodynamic properties. At adulthood, however, many nostoceratids develop a U-shaped hook, which indicates a shift in life habit during this growth stage (Peterman et al., 2020a,b,c).

73

74

75

76

77

78

79

80

81

82

83

84

85

86

87

88

89

90

91

92

93

94

95

Little is known about the soft body of ammonoids (Jacobs and Landman, 1993; Klug et al., 2012; Klug and Lehmann, 2015), but inferences can be drawn from their phylogenetic position and shell morphology. To move, ammonoids would have used jet propulsion through a soft-tissue tube called the hyponome. The shape and size of the hyponome can be inferred from a sinus built into the aperture. Some species (e.g. *Turrilites* costatus and T. scheuchzerianus) possess well-developed hyponomic sinuses, which may have allowed the hyponome to produce jet propulsion more efficiently in the downwards direction (Klinger, 1981). This feature suggests some torticones exhibited upward movement with active locomotion, either for vertical migration, or escape jetting (Klinger, 1981). Rostra, protruding from the venters of shells (e.g. those of some *Ostlingoceras*) are more enigmatic, but may have increased stability, protected the soft body, or propped the soft body away from the substrate. These features generally represent adult modifications, inferring that turrilitid life habit could have changed throughout ontogeny, even though the gross morphology of the shell remained constant. The sutural/septal asymmetry of turrilitids and other torticones suggest that the posterior soft body was asymmetrical (Ward, 1979a). The common occurrence of hyponomic sinuses and rostra suggest that the venter of the soft body at the aperture was positioned on the bottom of the shell (antapically). Therefore, the soft body was twisted in the body chamber since the siphuncle and adoral venter are located at two different positions on the whorl (similar to torsion occurring in gastropods).

Preserved mouthparts are rare in turrilitids. Atabekian (1987, Plate XIII, fig. 1e) reports aptychi (calcitic plates covering the lower jaws), which are similar in morphology to other Turrilitoid families (Tanabe and Landman, 2002; Kruta et al., 2009; Kruta et al., 2010). While there are likely morphological differences within this superfamily that indicate subtle differences in diet, turrilitids, like other ammonoids, were probably limited to feeding upon small organisms in the water column (Kruta et al., 2011; Keupp, 2012; Ritterbush, 2014).

Depth ranges of turrilitids

Some torticone species (e.g. *Turrilites costatus*) occur in many different facies. However, turrilitids are generally rare in northern portions of the Western Interior Seaway (Kennedy and Cobban, 1990), while more common in the south (Cobban et al., 2008) approaching neritic waters of the Atlantic Ocean. This facies independence, along with their absence in much of the Western Interior Seaway during the Cretaceous, suggests that some turrilitids were somewhat eurytopic, yet stenohaline (Kennedy and Cobban, 1976). Torticone ammonoids rarely preserve shell material adequate for isotopic analysis (Klinger and Kennedy, 1978), but well-preserved Cenomanian turrilitids from Australia were analyzed by Henderson and Price (2012). The authors compared oxygen isotope data of *Hypoturrillites* and *Turrilites* to contemporaneous benthic organisms, and interpreted a range of bottom-to-midwater depths for these helical ammonoids. Carbon isotopes from their study reveal that these species were likely sluggish with slow metabolic rates. Therefore, it is reasonable that turrilitids were generally nektobenthic to pelagic, with some taxa capable of vertically migrating in the water column (Ward, 1979a; Klinger, 1981) while passively searching for prey. Such life habits are generally in agreement with interpretations by Batt (1989) and Westermann (1996).

Turrilitids and the Cenomanian-Turonian Extinction

The most-successful clade of torticone-shelled cephalopods, Turrilitidae, went extinct during the Cenomanian-Turonian (C-T) crisis (Wright et al., 1996; Ifrim et al., 2015), which struck worldwide amidst a climatic re-organization of marine biogeochemical cycling (oceanic anoxic event OAE2 that occurred near the C/T boundary; Jenkyns, 1980; Arthur et al., 1987; Monteiro et al., 2012; Zheng et al., 2016; Jenkyns et al.,

2017). Ranking in the top-ten most severe biodiversity crises (Raup and Sepkoski, 1986), this mass extinction impacted marine microorganisms (calcareous nannoplankton, radiolarians, benthic and planktic foraminifera; Kaiho and Hasegawa 1994; Leckie et al. 2002; Elderbak et al. 2014), and marine animals at higher trophic levels (Elder 1989; Harries 1993; Harries and Little 1999; Monnet et al. 2003; Monnet and Bucher 2007; Monnet 2009; Jagt-Yazykova, 2012; Yacobucci, 2017). Turrilitid diversity was already on the decline before the OAE2, just after their peak in the middle Cenomanian (Monnet and Bucher, 2007; Monnet, 2009). Based on ammonoid diversity patterns, Monnet and Bucher (2007) questioned oceanic anoxia as the primary extinction mechanism for this event. Whether or not this pattern is supported (Kurihara et al., 2012; Giraud et al., 2013) or opposed (Hirano et al., 2000; Jagt-Yazykova, 2011), depends upon the taxa and paleogeographic areas of interest. Rare Turonian turrilitid occurrences are likely dubious (Klinger and Kennedy, 1978; Wright et al., 1996), and post-Cenomanian helical coiling primarily appears in the subadult stages of other turrilitoid families (e.g. Nostoceratidae), suggesting that this morphology still conferred adaptive advantages for other ammonoids. Understanding the physical capabilities and constraints on torticone ectocochleates would help elucidate how these cephalopods and other organisms responded to such global environmental changes.

Hydrostatics and Hydrodynamics in Ammonoids

The shape of ectocochleate cephalopod shells serve as an upper constraint on their locomotive abilities, life habit, and paleoecology (Ritterbush et al., 2014). Shell morphology strongly influences both hydrostatics (buoyancy, stability, orientation, and movement potential; Peterman et al., 2019, 2020a, 2020d), as well as hydrodynamics (drag, lift, and swimming aptitude; Peterman et al., 2020b, 2020c; Hebdon et al., 2020a, 2020b).

An ectocochleate is capable of neutral buoyancy when the sum of its organismal mass is less than, or equal to, the mass of water it displaces. Surplus buoyancy can be remediated by retaining small amounts of cameral liquid within the chambers (Hoffmann et al., 2015). The static life orientation occurs when the centers of buoyancy and mass are vertically aligned, and their separation imparts greater hydrostatic stability (Fig. 1A). Larger stability means that the orientation of the living cephalopod is less likely to be influenced by external

forces or swimming, but also restricts the manipulation of orientation with active locomotion (Peterman et al., 2019).

From a hydrostatics perspective, the directional efficiency of movement depends upon the relative positions of the source of jet propulsion (hyponome) and the center of rotation (occurring between the centers of buoyancy and mass; Fig. 1). The thrust angle (θ_t ; Fig. 1A) defines how much energy is transmitted into translational movement versus energy lost to rocking. When the hyponome and pivot point are horizontally aligned, more energy will be transmitted into backwards horizontal movement (Peterman et al., 2020a, 2020b, 2020c). When these two points are vertically aligned, vertical movement will occur with minimal rocking. The direction of thrust relative to the axis passing through the centers of mass and buoyancy is also important, especially for non-planispiral cephalopods like torticones. If the thrust vector is not aligned with this vertical axis, incident thrust will cause the cephalopod to rotate (Peterman et al., 2020a, 2020d). This angle (rotational thrust angle, θ_{tr} ; Fig. 1B) is measured between the thrust vector and the lever arm (L_x ; Fig. 1C) that connects the hyponome with the rotational axis. Idealized rotation would occur when thrust is applied perpendicular to the rotational axis ($\theta_{tr} = 90^{\circ}$), the thrust angle is 0° , and when the lever arm is large. Klinger (1981) and Ward (1979a) noted that rotation is likely to have taken place for torticones during jet propulsion.

The energy demands and physical efficiency produced by a twirling torticone are unknown.

Furthermore, shell shape suggests that passive rotation would occur during vertical movement; the prospect of rotation is fundamental to torticone locomotion. Ornamentation may exacerbate rotation but, like other features of torticone shells, is not well-constrained by simulations or experiments. We investigate the hydrostatic and hydrodynamic properties of the torticone morphotype with virtual and physical models of the turrilitid, *Mariella brazoensis*. While the potential life habit for torticone ammonoids likely varied, these experiments provide insights into the rotational capabilities of this morphotype and the biomechanical relationships that would have constrained the behavior and ecology of these helically-coiled ammonoids.

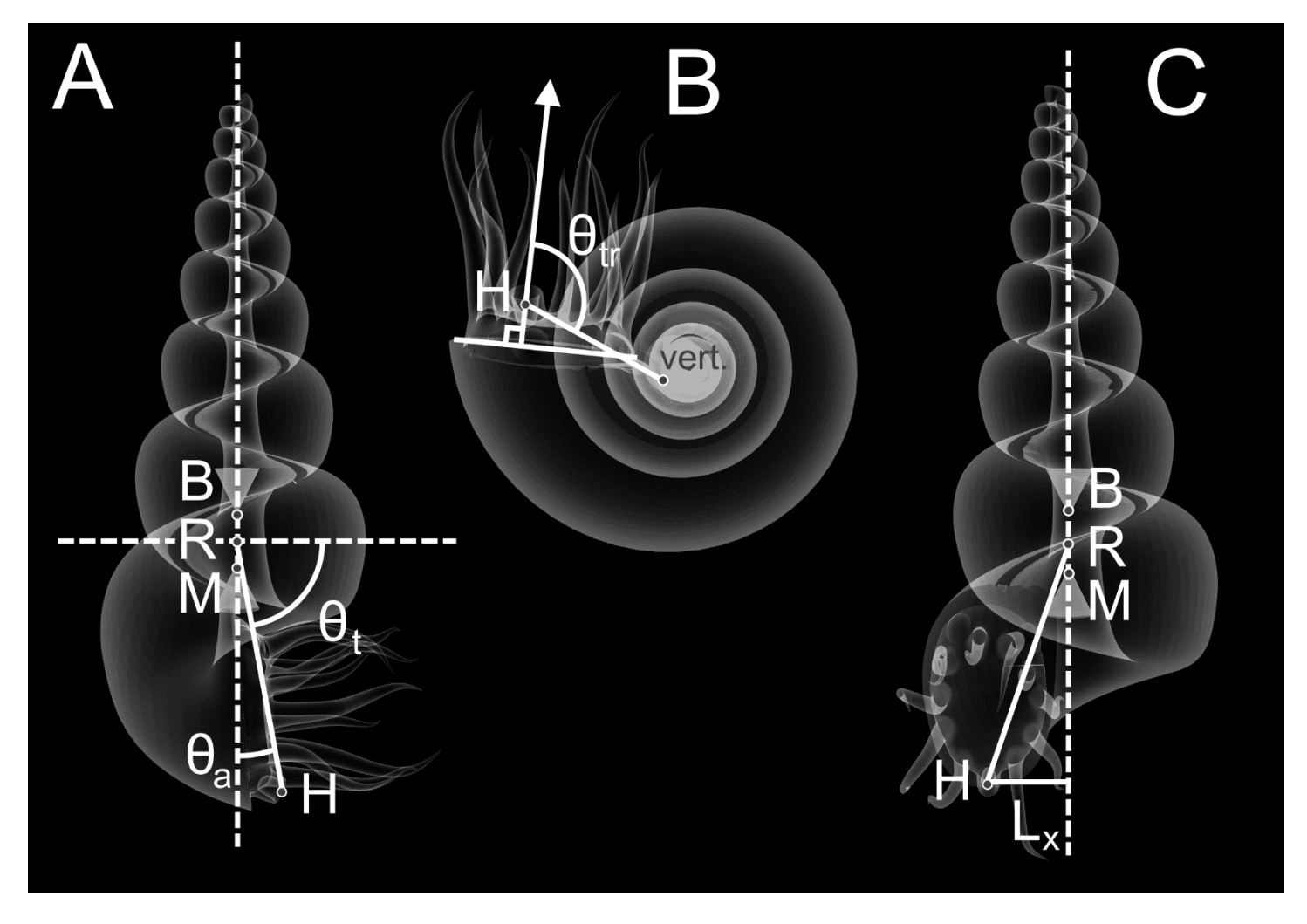


Figure 1: Hydrostatic measurements of torticones. A) Side view in life orientation showing the measurement of the apertural angle (θ_a), and thrust angle (θ_t). B) Vertical view, depicting the measurement of the rotational thrust angle (θ_t). C) Front view, denoting the lever arm (L_x) that produces torque during jet propulsion. B = center of buoyancy, M = center of mass, R = horizontal rotation pivot point, H = hyponome, source of jet thrust.

METHODS

Virtual and physical reconstructions of the torticone models follow the methods of Peterman et al., (2020b, 2020c), with some modifications described below. For turrilitids, such methods are preferred over tomographic techniques (Hoffmann et al., 2014, 2018; Tajika et al., 2015; Lemanis et al., 2015; Naglik et al., 2015b, 2016; Inoue and Kondo, 2016) due to the rarity of well-preserved shell material for this family (Kennedy and Cobban, 1976; Klinger and Kennedy, 1978; Kennedy et al., 2005). To investigate the syn vivo physical properties of the torticone morphotype, models were constructed for the species *Mariella* (*Wintonia*)

brazoensis (Roemer, 1852). A smooth version of this morphology with a simple, elliptical whorl section was constructed to assess the hydrodynamic influences of shell ornamentation.

Virtual Modeling

180

181

182

183

184

185

186

187

188

189

190

191

192

193

194

195

196

197

198

199

200

201

202

The external shell of *Mariella brazoensis* was constructed in the program Blender 2.79 (Blender Online Community, 2017) with array algorithms (Table 1). These instructions build the external shell by replicating the adapertural whorl section while simultaneously translating, rotating, and scaling. This method can be used to build theoretical shells, similar to those of Raup (1967), although the shell is built from the aperture to apex. After the whorl sections were replicated, they were bridged together to create a tessellated mesh of a smooth shell. The values of this array were chosen by digitizing an image of Mariella brazoensis to use as a stencil (USNM 520221, National Museum of Natural History - Smithsonian Institution; Kennedy et al., 2005, fig. 50E). A single array that approximates this shell morphology was fit by eye. The original scale of this model was arbitrarily increased to limit the influence of round-off in the array instructions. Ornamentation for this species was 3D modeled with photogrammetry of USNM 430965. Fifty photographs were used to construct a 3D model of this specimen in the program 3DF Zephyr (3DFLOW, 2018). A single pattern of the shell ornamentation with three rows of tubercles and a lateral groove between the lower two rows was extracted from the photogrammetry model. This ornamented section of shell was placed on the smooth version and replicated with the same array instructions used to build the shell (Table 1). Extraneous sections were deleted to approximate the spacing between neighboring tubercles (as indicated by the original photogrammetry model). Shell thickness was approximated as a ratio of whorl height by measuring an image of *Mariella bergeri* (Brongniart, 1822) of specimen GS G183 (Geological Collections, Faculty of Culture and Education, Saga University, Saga, Japan) from Matsumoto and Kawashita (1999). The shell thickness to whorl height ratio for this specimen was measured at 0.03. While measuring a photograph with somewhat oblique views was crude. this measurement closely aligns with the value used for the turrilitoid, *Didymoceras* in Peterman et al. (2020a),

which is the same after rounding to the second decimal place. Each ornamented, replicated segment was extruded (defined thickness) according to this ratio.

Table 1: Array instructions used to build the shell of *Mariella brazoensis*. Large, arbitrary initial dimensions were used to avoid round-off error. The initial whorl section, originally modeled as a simple ellipse (maximum and minimum dimensions shown), was translated, rotated, and scaled in the x, y, and z directions to build the shell from the aperture to the apex. The center of the initial whorl section serves as the datum for these transformations. Shell ornamentation and septa were also replicated with these instructions.

	X	y	Z
Translation (mm)	-46.090	-4.200	-5.370
Rotation (degrees)	0.3	-6.1	0.1
Scale	0.994	0.995	0.996
Whorl Section Size (mm)	88.788	129.806	0.000
Whorl Section Center (mm)	-46.804	-6.295	0.800

Due to the lack of well-preserved shell material for *Mariella brazoensis*, the suture pattern of, *Mariella bergeri* was used to model the septa (recorded in Ward, 1979a, fig. 3A). Septal morphology does not substantially vary between this species and *M. brazoensis*. This suture pattern allows for the appropriate septal spacing (therefore number of modeled septa) to be determined. The *M. bergeri* suture pattern was converted to a 3D object, then wrapped around the whorl section and extruded inwards to a single point in its center. The periphery of the septa was confined to the shape of the shell by using the "magnetize" tool in Meshmixer 3.3 (Autodesk Inc., 2017a). The internal portions of the septa (excluding the suture pattern) were selected and progressively smoothed to approximate a minimum curvature surface (Peterman et al., 2020c, 2020d). Septa were extruded based on the septal thickness to whorl height ratios for *Didymoceras* (0.01) measured in Peterman et al. (2020a). The extruded septa were replicated with the same array instructions used to build the shell. Extraneous septa (seven septa in between every two) were deleted so that their lobules and folioles were almost touching.

The proportions of the body chamber are poorly documented for turrilitids. Trueman (1941) depicts a torticone body chamber somewhere in between 1.5 to 2 whorls, which is similar to body chamber lengths in Klinger (1981). Torticones with lower whorl expansion (like *Ostlingoceras*) likely have larger body chamber ratios (by number of whorls) than squat forms like *Hypoturrilites* to maintain similar proportions by volume. Slowly tapering, orthoconic cephalopods like baculitids have body chamber ratios of 40% their total length (Peterman et al., 2019). If a baculitid shell was coiled into the helical shape of *Mariella brazoensis*, this value translates to a little more than 1.5 whorls, which aligns with Trueman (1941) and Klinger (1981). The curvilinear length of the body chamber was computed in Blender so that it was equal to 40% of the total curvilinear length. This ratio determined the position of the terminal septum that separates the phragmocone from the body chamber.

The final shell was constructed by unifying the 3D mesh of the septa with the 3D mesh of the shell in the program Netfabb 2017.3 (Autodesk Inc., 2017b). This program was also used to repair meshes into manifold objects that are suitable for volumetry. To compare the hydrodynamic role of ornamentation (described below), a smooth-shelled model with a simple, elliptical whorl section was constructed with the same methods and model proportions. These virtual models of torticone shells were then scaled the approximate size of USNM 520221 (longest axis dimension of 15 cm).

The soft body was constructed by isolating the internal interface of the body chamber from the shell model. The normals of this interface (which denote the exterior direction) were reversed so that they were appropriately pointing outwards. A soft body resembling the consensus of Klug and Lehmann (2015) was placed at the aperture of the model. Previous studies (Peterman et al., 2019, 2020d) have demonstrated that the hydrostatic influences of the assumed soft body morphology are minimal as long as their volumes are reasonable. Cameral volumes are also required for buoyancy calculations. These volumes were extracted from the phragmocone by deleting the external shell, allowing the cameral volumes to be isolated and their faces inverted. The volume and distribution of water displaced are required for each hydrostatic calculation. This

model was created by isolating the external mesh of the shell and soft body and then deleting the interior. All meshes were then repaired in Netfabb 2017.3 (Autodesk Inc., 2017b) to create closed, manifold 3D objects. All volumes and centers of mass for these 3D models were computed in MeshLab (Cignoni and Ranzuglia, 2014).

Calculation of Hydrostatic Properties

For a more extensive explanation of the hydrostatic calculations and their physical relationships see Okamoto (1996), Hoffmann et al. (2015), and Peterman et al. (2019, 2020d). The capacity for neutral buoyancy (Φ) is defined here as the proportion of the phragmocone to be emptied of cameral liquid that would allow a neutrally buoyant condition to persist (Peterman et al., 2019):

$$\Phi = \frac{\left(\frac{V_{\text{wd}}\rho_{\text{wd}} - V_{\text{sb}}\rho_{\text{sb}} - V_{\text{sh}}\rho_{\text{sh}}}{V_{\text{ct}}}\right) - (\rho_{\text{cl}})}{(\rho_{\text{cg}} - \rho_{\text{cl}})} \tag{1}$$

Where V_{wd} and ρ_{wd} are the volume and density of the water displaced, V_{sb} and ρ_{sb} are the volume and density of the soft body, V_{sh} and ρ_{sh} are the volume and density of the shell, ρ_{cl} is the density of cameral liquid, ρ_{cg} is the density of cameral gas, and V_{ct} is the total cameral volume of the phragmocone. A soft body density of 1.049 g/cm³ is preferred based on bulk density calculations which include *Nautilus*-like tissues (Hoffmann and Zachow, 2011), a seawater-filled mantle cavity, and thin aptychi (Peterman et al., 2020b). A shell density of 2.54 g/cm³ (Hoffman and Zachow, 2011), cameral liquid density of 1.025 g/cm³ (Greenwald & Ward, 1987), and cameral gas density of 0.001 g/cm³ are used here.

The centers of mass of the soft body, shell, cameral liquid, and cameral gas were computed in MeshLab (Cignoni and Ranzuglia, 2014). Due to the low density of the cameral gas, and low volume of the cameral liquid, the centers of these two materials were set equal to the center of volume of the camerae. The total center of mass was computed with the following equation:

$$M = \frac{\sum (L*m_o)}{\sum m_o} \tag{2}$$

Where M is the total center of mass in a principal direction, L is the center of mass of a single object measured with respect to an arbitrary datum in each principal direction, and m_o is the mass of any particular object that

has a unique density. Equation 2 was used in the x, y, and z directions to compute the coordinate position of the center of mass. The center of buoyancy (B) was found by computing the center of volume of the model representing the displaced water.

The static orientation of the total model occurs when B and M are vertically aligned. The hydrostatic stability index is computed from these two centers.

$$S_t = \frac{|B-M|}{\sqrt[3]{V}} \tag{3}$$

The separation between the centers of buoyancy (B) and mass (M) is normalized by the cube root of the organismal volume (V; equal to the volume of seawater displaced).

Apertural angles (θ_a) were measured with respect to the vertical (Fig 1A). That is, angles of zero correspond to a horizontally facing soft body, angles of +90° correspond to an upwardly facing soft body, and angles of -90° correspond to a downwardly facing soft body.

Thrust angles (θ_t) were measured from the horizontal (Fig 1A) between the point source of thrust and the rotational axis. Therefore, as the thrust angle approaches zero, more energy is transmitted into horizontal movement with a lower rotational component. As thrust angles approach -90°, energy would be optimally transmitted into upwards movement.

Rotational thrust angles (θ_{tr}) were measured between the thrust vector (perpendicular to the aperture) and the rotational axis (Fig 1B). A rotational thrust angle of 90° would allow pure rotation to take place, while angles of 0° and 180° would result in translational movement. This thrust vector was likely able to be modified by the living animal through repositioning the hyponome.

Computational Fluid Dynamics Simulations

Hydrodynamic drag and the trajectory of incident streamlines were computed with computational fluid dynamics (CFD) simulations in the software, ANSYS Fluent 2018 (ANSYS Inc., 2018). Simulations were performed under steady state conditions at 10 cm/s (2/3 body length per second) with fluid flow in the downward direction, upward direction, and horizontal (adoral) direction. While downward movement is likely

to occur from a subtle negative buoyancy (like extant *Nautilus*; Ward and Martin, 1978; Ward, 1979b) rather than active locomotion, its velocity was held at the same value as the other movement directions to compare the differences between them. To follow the physical experiments, the torticones with smoothed soft bodies were used. Shells were modeled as stationary objects within the fluid domain following Hebdon et al. (2020 a,b). While the influence of this assumption is lower for bilaterally-symmetric, planispiral ectocochleates, they still allow relative forces of drag in the principal directions to be compared for torticones. Therefore, relative forces of drag and their x, y, and z components were compared between each simulated flow direction instead of computing drag coefficients.

For each simulation, the rectangular fluid domain was meshed using primarily tetrahedral elements with layers of prism elements directly surrounding the shell to capture near wall boundary behavior. Two rectangular zones of refinement were used within the domain. The first zone had a maximum element size of 0.001 mm and was centered around the shell. The second had a maximum element size of 0.005 mm and was placed behind the shell (according to flow direction). These finer element zones were used to capture the flow fields of interest (those directly affected by the shell). We allowed the element size of the remaining regions to be controlled by the meshing program. The resulting meshes had between 14.8 and 14.9 million elements with horizontal flow directions generally having a higher element count than the vertical flows. The size of the fluid domain was 30 by 30 by 70 cm. The longest axis belongs to the flow direction for each simulation.

Simulation settings follow the methods of Hebdon et al. (2020b). Each simulation used the Reynolds Averaged Navier-Stokes solver and the Shear Stress Transport (SST) k- ω model was used for turbulence closure. Velocity was set at the inlet with a constant zero pressure at the outlet. The walls were given the symmetry condition to any potential impact on flow around the shell. The boundaries of the shell were given the no-slip condition and Fluent's default liquid water settings were used to set the fluid density and viscosity.

Constructing 3D Printed Models for Physical Experimentation

Several physical models were constructed by 3D printing geometries that maintained the hydrostatic properties (Fig. 2A and B) of their corresponding virtual models (following the methods of Peterman et al., 2020b, 2020c). All models were printed with PLA (polylactic acid) filament with an Ultimaker S5, 3D printer. A soft body with rigid arms would unrealistically influence hydrodynamics during movement. To prevent this, a smooth soft body was constructed while maintaining the volume of displaced water (to the nearest 0.0005 cm³). Unlike the virtual model, the physical experiments were performed in tap water, so their masses were adjusted accordingly. The density of the tap water was measured with a 100 ml pycnometer at 0.9998 g/cm³. Four models were constructed to simulate upwards movement and downwards movement for a shell with ornamentation and without ornamentation. Watertight voids were constructed over 10 to 13 iterations. These voids, along with coiled, steel wire counterweights, adjusted the mass distribution to maintain hydrostatic stability and the static orientation. Counterweights were designed to fit in the internal portion of the spiral to be interchangeable (Fig. 2C and D). This design allowed two different counterweights to be used for each model. which simulated *Nautilus*-like and coleoid-like thrust, respectively. *Nautilus*-like thrusts (1047 dynes) were computed from scaling the maximum average thrust (0.12 N) required for an adult *Nautilus* (1.6 Kg) to overcome drag at its maximum swimming speed (25 cm/s) to the mass of the torticones (0.141 Kg). A coleoidlike thrust (2670 dynes) was chosen, which falls in between the thrusts of Sepia officinalis and Loligo vulgaris after scaling by their relative mantle cavity volume to total volume ratios (Nautilus = 0.15; Sepia officinalis = 0.25; Loligo vulgaris = 0.5; Chamberlain, 1990). Each of these thrusts are the result of mass surpluses and deficiencies, resulting in artificial positive and negative buoyancy. In reality, the thrust of the living ammonoids would have oscillated, with each pulse falling from higher peak thrusts to overcome drag. Downwards movement of the living ammonoid would be more consistent with the physical experiments since it would likely result from slight negative buoyancy rather than active locomotion. Therefore, the values used in this study represent continuous thrusts required to overcome drag at maximum swimming velocity estimates of their extant analogues, which are held constant in each direction for comparison.

318

319

320

321

322

323

324

325

326

327

328

329

330

331

332

333

334

335

336

337

338

339

340

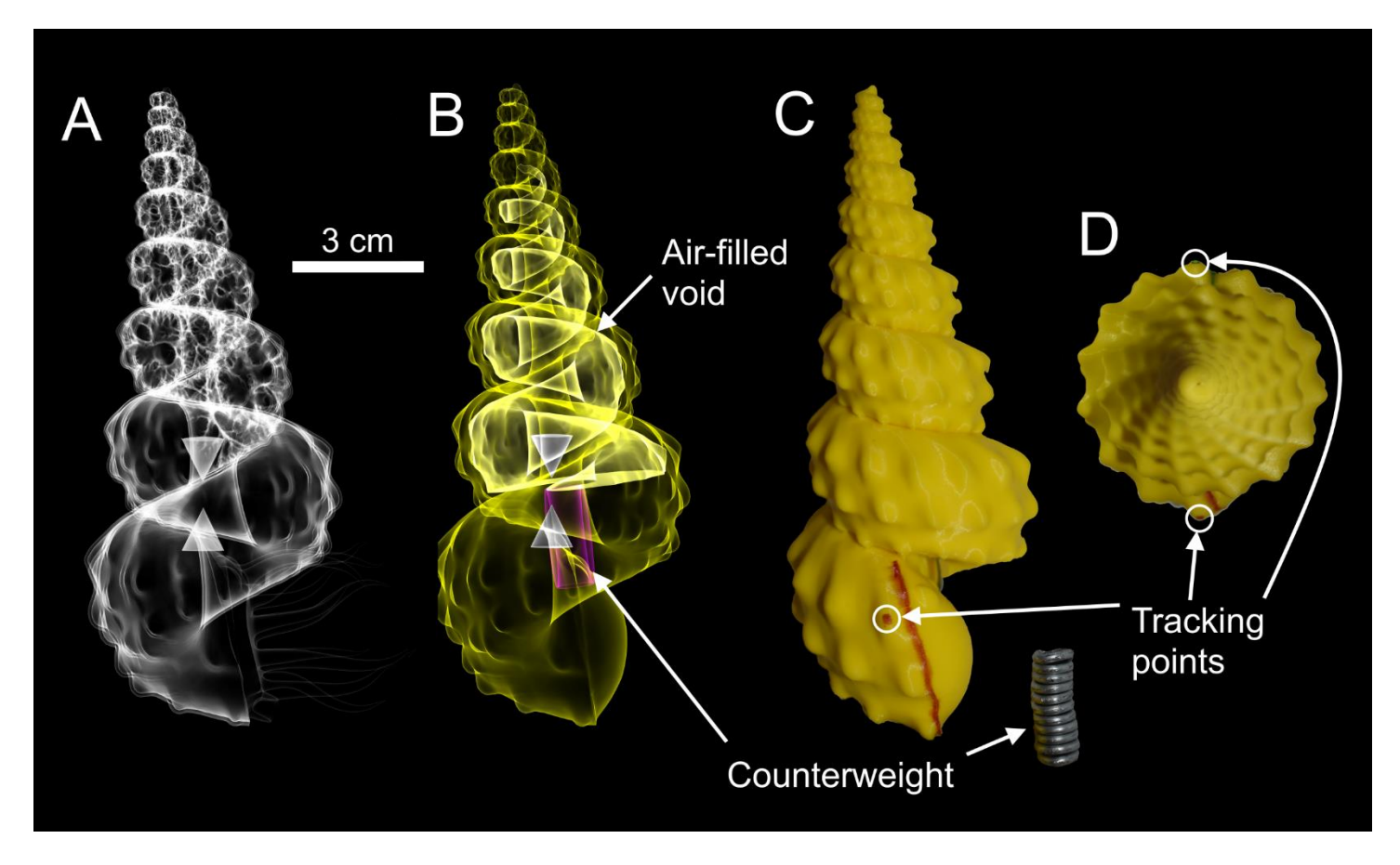


Figure 2: Construction of a 3D printed torticone model for physical experimentation. A) Virtual hydrostatic model with complex internal geometry and nonuniform density, both of which govern the mass distribution. The points of the upper cone and lower cone correspond to the centers of buoyancy and mass, respectively. B) Virtual model simplified for printing, while maintaining the mass distribution of the complex hydrostatic model. An air filled void and steel wire counterweight correct for the differences in mass and its distribution, and allow the model to be 3D printed in uniform density PLA (polylactic acid) filament. C) 3D Printed torticone model. D) Top view showing the location of the tracking points used to determine angular displacement, angular velocity, and angular acceleration.

Passive rotation, occurring as a consequence of vertical movement through water, was monitored in a 50-gallon tank, filled with 70 cm of water in the vertical direction. A release mechanism was used to position the positively and negatively buoyant models at the bottom and top of the tank, respectively. Video footage was recorded at 2.7k resolution at 24 frames per second with a GoPro Hero 7 that was mounted above the tank on brackets. Four columns of waterproof LEDs lined the tank to provide an even gradient of light at various depths.

The relative angle was computed from the position of two tracking points placed on the model – one near the aperture, and the other half of a whorl (180°) from the aperture (Fig. 2D). Tracking points were monitored in the program Tracker 4.11.0 (Brown, 2017). The X and Y coordinates were used to compute their relative changes in angle (angular displacement) and angular velocity as a function of time. A total of eight different experiments were performed with 13 to 15 trials each (combinations of ornamented and smooth models, moving in the upward and downward directions, at *Nautilus*-like thrusts and coleoid-like thrusts).

A neutrally buoyant model was also constructed to measure the model's resistance to rotation. Fifteen trials were performed at various initial velocities and monitored with the motion tracking software. The difference in angle from the starting location (angular displacement) as a function of time was fit with an asymptote equation in the form:

$$\theta(t) = \frac{(at)}{1+bt} \tag{4}$$

where θ is the relative angle between the two tracking points, a and b are coefficients, and t_i is time at a given timestep. This equation was fit in MATLAB with the curve fitting toolbox, then differentiated within the same program to compute angular velocity and angular acceleration.

The net torque on the model during rotation was found by multiplying the computed angular acceleration (in radians) with the moment of inertia. The moment of inertia was computed in MeshLab (Cignoni and Ranzuglia, 2014) after translating the model so that the axis passing through its centers of buoyancy and mass was coincident with the origin. The vertical axis moment had to be normalized by the mesh volume and its units corrected (to $Kg*m^2$) to find the appropriate value.

During ventilation of the gills, extant *Nautilus* produce about 80 dynes of thrust (based on speeds of a 1.6 kg individual; Wells and O'Dor, 1991). This translates to a thrust of 6.46 dynes after scaling to the mass of the torticone models. This ventilation thrust was used as an estimate for the ease/difficulty in sustaining low angular velocity rotation. This value was multiplied by the lever arm from the rotational axis to the hyponome (2.04 cm) to compute the torque imparted on the model during ventilation of the gills. The torque induced by

ventilation was compared with the torque resulting from the model interacting with the surrounding fluid to determine if any substantial amount of rotation could be sustained.

RESULTS

Hydrostatic properties of Mariella brazoensis

The hydrostatic model with a 40% body chamber length to total length (around 1.5 whorls) is capable of neutral buoyancy by emptying 84.7% of its chamber volumes of liquid (Fig. 3; Table 2). Increasing the body chamber to two whorls (a ratio of ~50% by length) results in negative buoyancy (Φ = 119%). The shell is oriented apex-upwards with the soft body facing almost horizontally (θ_a = 12.3°; Table 2). The coiling axis of the shell is slightly displaced from the vertical (8°) due to the influence of the expanding body chamber on the distribution of mass. This orientation is stable, with a hydrostatic stability value (S_t = 0.122; Table 2) over twice that of *Nautilus* (0.05; Peterman et al., 2019).

Shell thickness is difficult to measure for turrilitids because of the rarity of shell preservation. The influence of this parameter was tested by increasing and decreasing the total shell volume by 15% yielding Φ values of 104% and 65.3%. This suggests that a nearly neutral buoyancy would still take place even if the shell thickness was increased by 15%. The volume of the soft body is much more influential on hydrostatics, being over six times that of the shell. The models are also somewhat sensitive to the density values used. Increasing the shell density to historically higher values (2.67 g/cm³; for review, see Hoffmann et al., 2015) slightly increases the percentage of cameral gas in the phragmocone ($\Phi = 91.4\%$).

Table 2: Hydrostatic properties of the ornamented and smooth *Mariella brazoensis* models. Φ = conditions for neutral buoyancy (i.e., the percentage of the phragmocone to be emptied of cameral liquid). S_t = hydrostatic stability index. θ_a = apertural angle. θ_t = thrust angle. θ_{tr} = rotational thrust angle. Measurements further defined in Figure 1.

	Ornamented	Smooth
Percent gas in phragmocone (Φ)	84.7	79.9
Hydrostatic stability index (St)	0.122	0.116
Apertural orientation (θ_a)	12.3°	10.6°

Thrust angle (θ_t)	-74.1°	-76.2°
Rotational thrust angle (θ_{tr})	110.1°	112.5°

The location of the hyponome is much lower than the horizontal rotational axis (Fig. 3A and 3C), resulting in a thrust angle that is poor for the efficient transmission of thrust energy into horizontal movement ($\theta_t = -74.1^{\circ}$). The same amount of thrust would result in better upwards vertical movement than horizontal movement, because less energy would be lost to rotation about the midpoint between the centers of buoyancy and mass (Fig. 3C). The rotational thrust angle would result in aperture-backwards rotation about the vertical axis if thrust is produced at the hyponome ($\theta_{tr} = 110.1^{\circ}$).

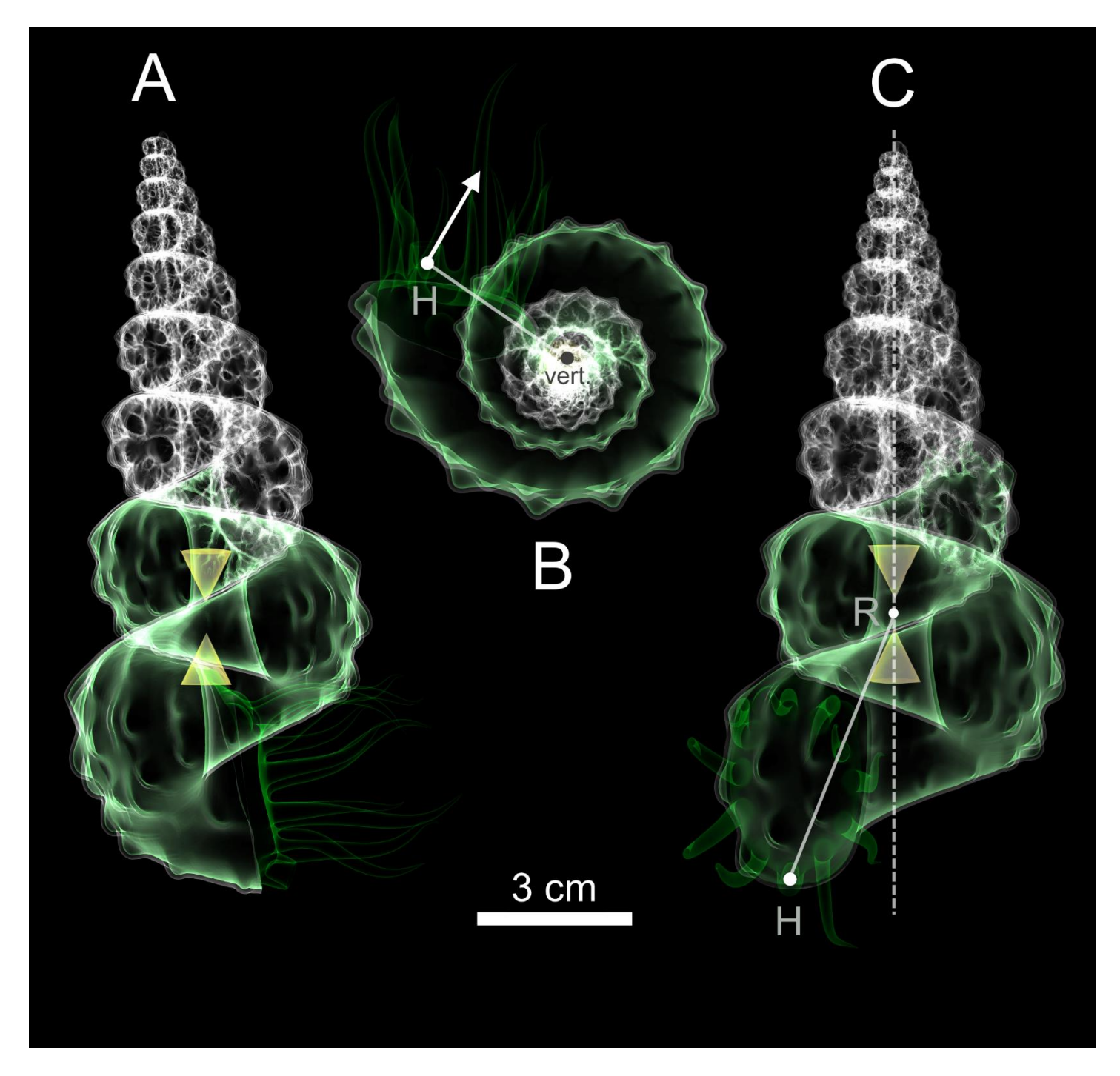


Figure 3: Final hydrostatic models of *Mariella brazoensis* oriented according to their life position. A) Side view. B) Vertical view showing the ideal direction of thrust for pure rotation. C) Front view. The points of the upper and lower cones correspond to the centers of buoyancy and mass, respectively. R = pivot point for rotation about some horizontal axis, H = location of hyponome, source of jet thrust, Dashed line = vertical rotation axis.

The smooth torticone model (Fig. 4) has similar hydrostatic properties to the ornamented one representing *Mariella brazoensis* (Table 2). By removing ornamentation and slightly changing the whorl

section, mass and its distribution are subtly altered. However, the primary purpose of this model was to investigate the differences in hydrodynamics (described below).

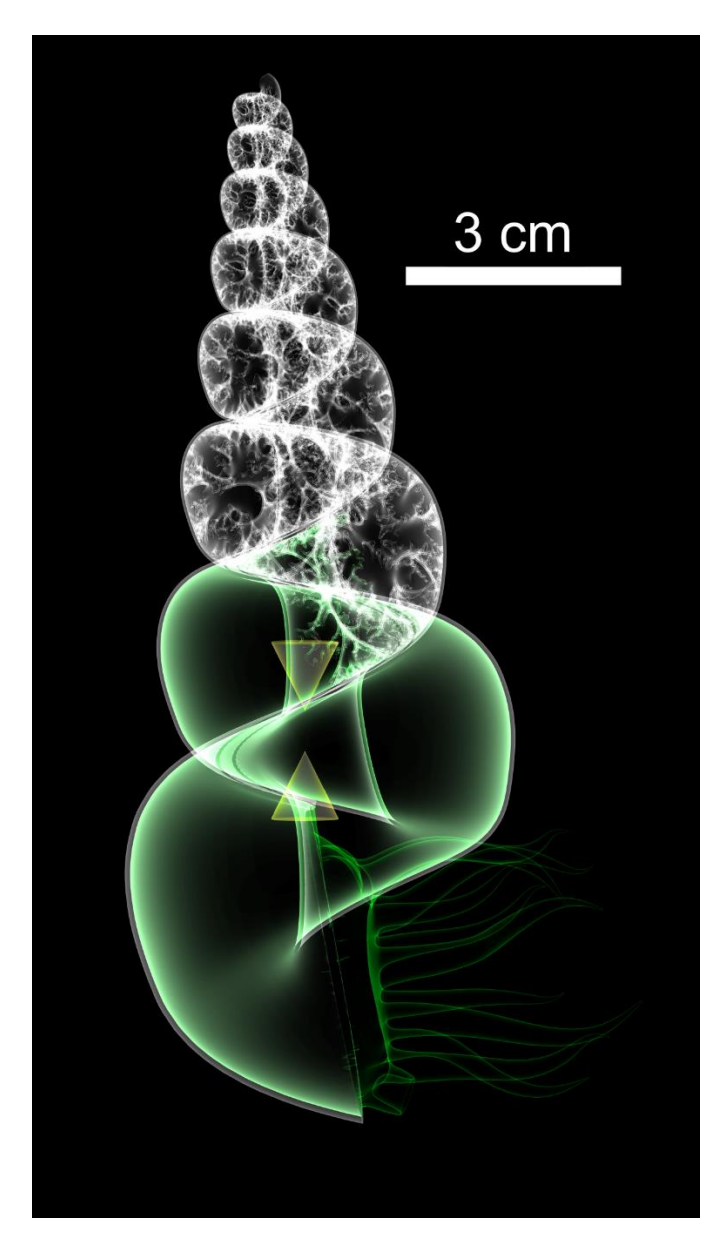


Figure 4: Smoothed version of the hydrostatic model of *Mariella brazoensis*. The points of the upper and lower cones correspond to the centers of buoyancy and mass, respectively.

Due to the minor changes in coiling throughout ontogeny, it is unlikely that these hydrostatic properties would change for most of the lifetime of these ammonites. Hydrodynamics, however, depend upon size.

Juvenile torticones would have had experienced larger relative viscous forces due to their smaller size (and therefore smaller Reynold's Number). Such changes in scale were not investigated in the current study.

Computational Fluid Dynamics Simulations

Small proportions of the streamlines follow the contours of the stationary shell, however, fluid flow over the last whorl appears to have the largest influence on rotation. This behavior suggests that rotational movement would occur if the torticone was able to move freely (which is observed in the later described physical experiments). During upward movement (downward flow direction) the incident streamlines rotate in the direction of shell growth (Fig. 5), which would cause the torticone to rotate aperture-backwards in a non-stationary setting. The opposite direction of rotation is inferred from the pressure gradients on the underside of the shell during downward movement (upward flow direction; Fig. 6). Incident streamlines first encounter the adapertural shell, then move opposite of the shell's growth direction. Since the later whorls encountered by incident flow are smaller, turbulence is formed in these areas, contributing some rotation in the same direction. Although, some of the streamlines are directed in a similar direction to the upward movement simulation. This relationship is more complicated than upwards movement, but yields a net torque producing aperture forward rotation (as observed in the physical experiments). The arms of the living cephalopod could have disrupted flow, depending on their orientation and morphology. However, their influence would be lower than that of the rigid shell.

The x and y (horizontal) components of drag during vertical movement also agree with the movement directions inferred from the subtle rotation of the streamlines (Table 3). The y components are positive for the simulation of upward movement, yielding aperture-backward rotation. This same component is negative for the downward movement simulation, imparting aperture-forward rotation. The z components of drag experienced by the models during vertical movement and the x component of drag during horizontal movement allow a comparison of the relative resistance to movement through fluid in each direction. Horizontal movement yields much more drag in this direction than the models experiencing vertical movement, which would require the

living cephalopods to generate larger thrusts to obtain the same effective velocities. Upwards vertical movement incurs the least amount of drag, while downward movement is only slightly higher. This vertical streamlining of torticones is depicted in Figure 7 with velocity cross-sections.

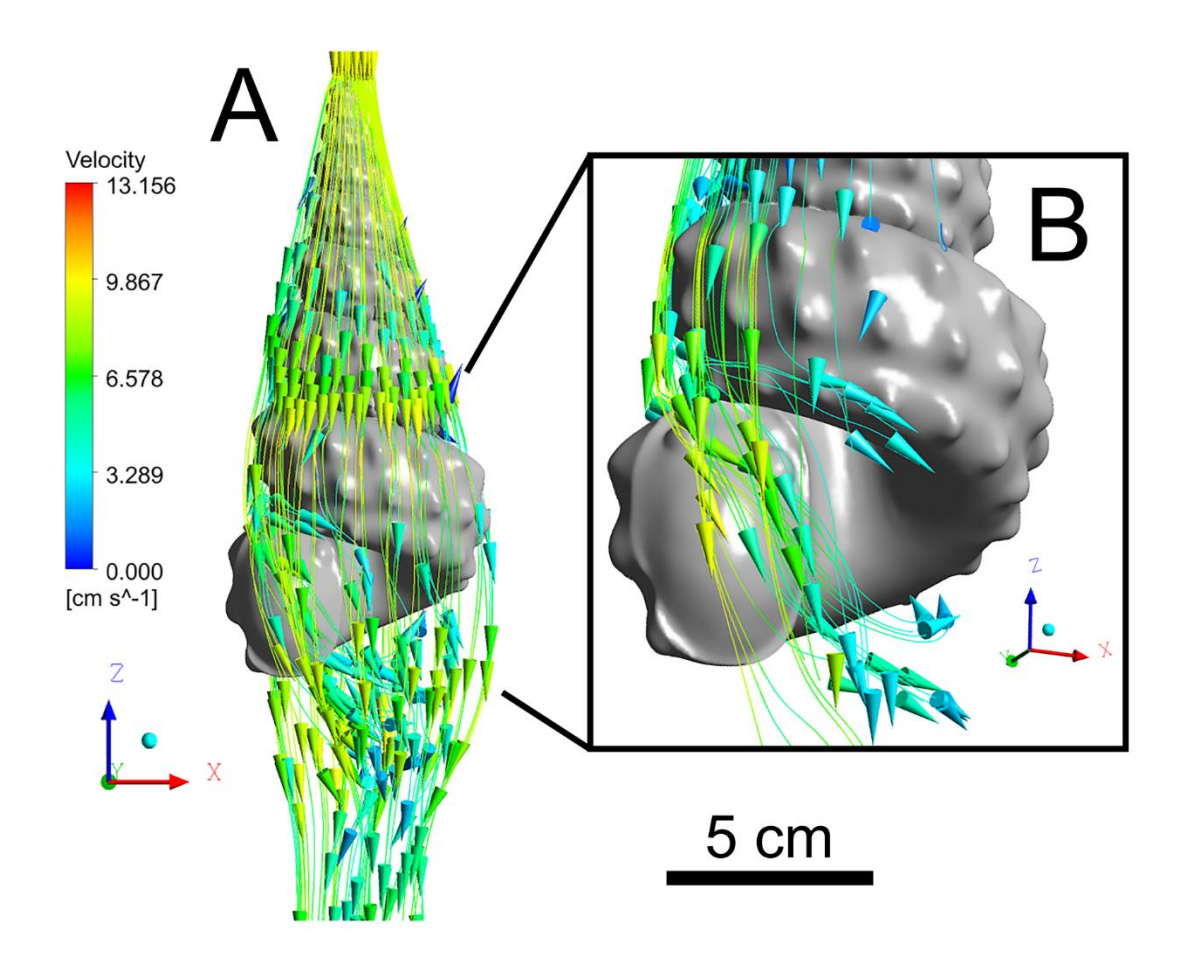


Figure 5: Results of computational fluid dynamics (CFD) simulations showing streamlines passing over the torticone model. A) Torticone moving in the upward direction at 10 cm/s. B) Enlarged view drawing attention to rotating streamlines. Arrows denote the relative flow direction of the fluid.

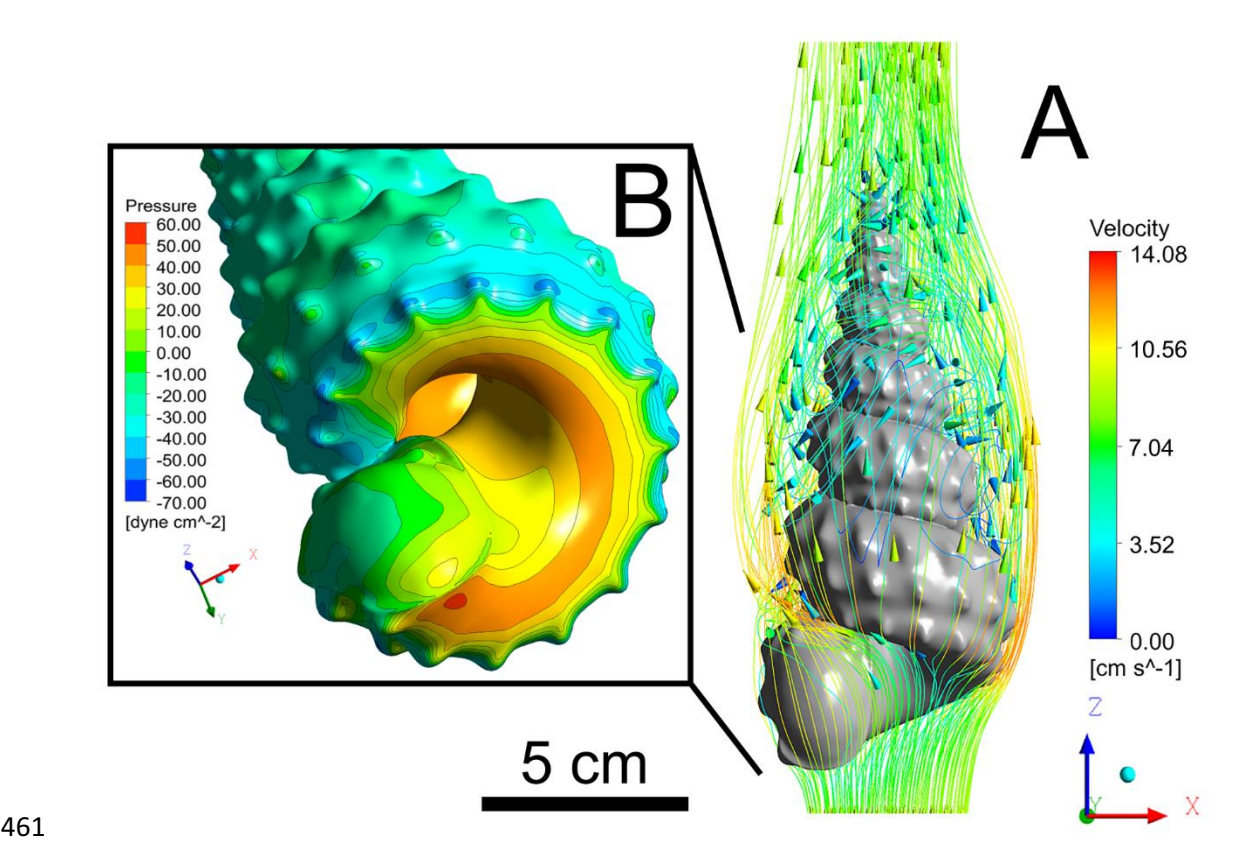


Figure 6: Results of computational fluid dynamics (CFD) simulations showing streamlines passing over the torticone model. A) Torticone moving in the downward direction at 10 cm/s. B) Enlarged view showing pressure contours along the underside of the shell. Arrows denote the relative flow direction of the fluid.

Table 3: Hydrodynamic drag forces computed during computational fluid dynamics simulations in the upward, downward, and horizontal directions of movement. The x, y, and z components of drag force are reported from two velocities within the range of the physical experiments. Bold numbers refer to drag forces occurring in the direction of movement.

Movement	Flow	Flow	F _{dx} (dyn)	F _{dy} (dyn)	F_{dz}
Direction	Direction	Velocity			(dyn)
		(cm/s)			
Upwards	-Z	5	-18.65	-32.15	-166.06
Upwards	-Z	10	-34.86	-196.76	-659.34
Downwards	+z	5	-16.71	84.33	206.56
Downwards	+z	10	-48.22	291.91	809.23
Horizontal	$+_{\mathbf{X}}$	5	549.79	63.38	-151.68
Horizontal	+ x	10	2223.48	313.38	-608.59

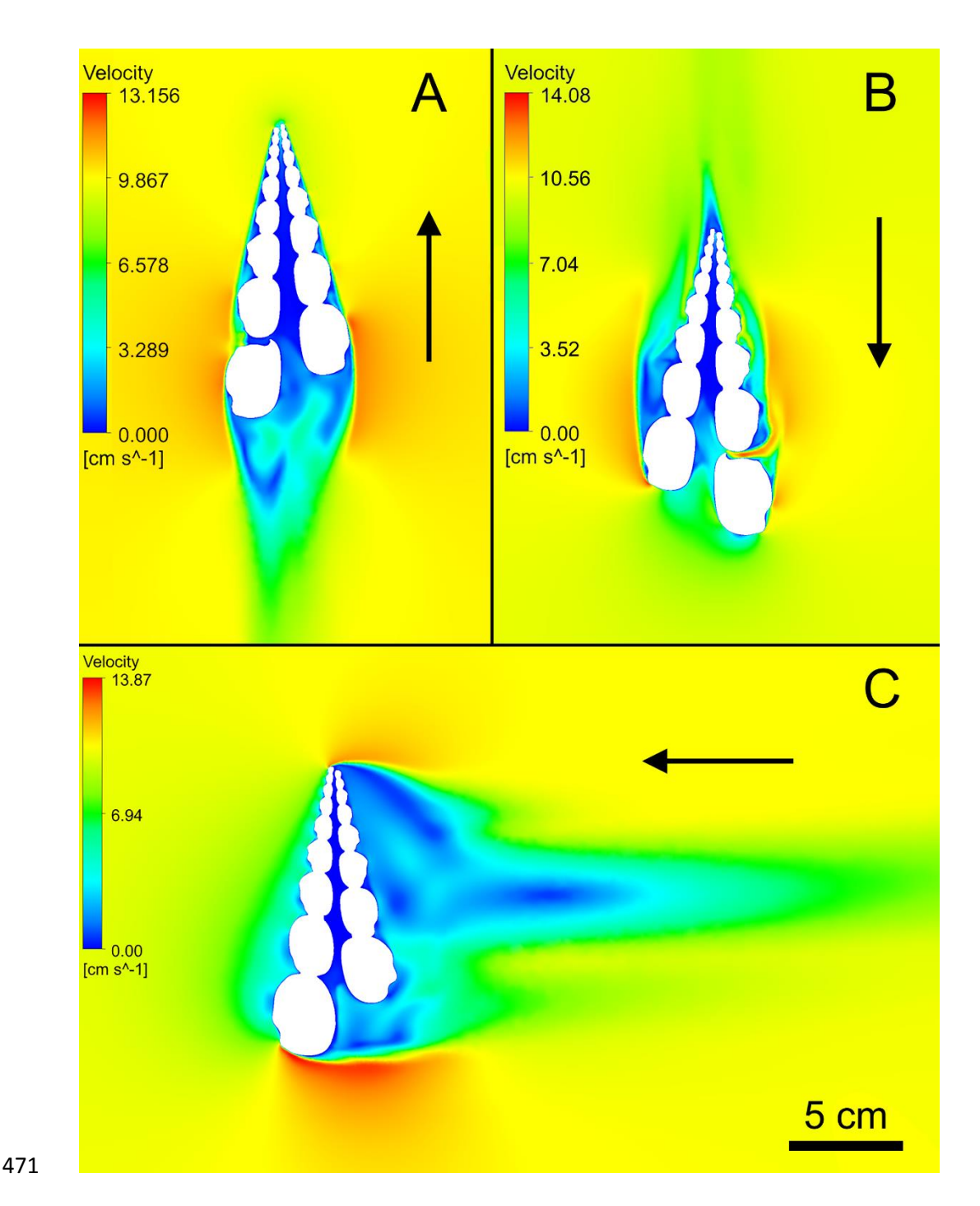


Figure 7: Computational fluid dynamics simulations showing cross sections of the models and the surrounding fluid velocity within this plane. Arrows denote movement direction of the torticone. A) Upward movement. B) Downward movement. C) Horizontal movement (aperture-backwards direction). Movement in the vertical directions is more streamlined, while the horizontal direction produces more hydrodynamic drag.

Physical Experimentation on Vertical Movement

Nautilus-like estimates of thrust cause the 3D printed models to rotate during both upwards and downwards vertical movement (Fig. 8A). During upwards movement, the models rotate aperture-backwards (positive angular displacement). In contrast, downwards movement causes aperture-forward rotation (negative angular displacement). Coleoid-like thrusts result in quicker vertical movement as well as larger angular velocity and angular acceleration (Fig. 8C and D). During upwards movement with these larger thrusts, the coiling axis of the shell undergoes more precession. At these higher thrusts/velocities, the apex tilts further from its static orientation during upwards movement and the entire shell begins to translate in the direction of the aperture during downwards movement. These different forms of movement are responsible for the deflections most easily viewed in the angular velocity plots (Figs. 8B and 8D). Difference in angular displacements and angular velocities between the ornamented and smooth models are likely the result of discrepancies in mass and/or volume, causing some deviation from the target buoyancy values (errors reported on Table 4). Angular velocities should ideally start at zero if the initial conditions are perfectly static. However, time zero was defined as the moment the release mechanism left the models, and in some trials, the models were already weakly in motion before they left this mechanism.

Table 4: Error in thrust values for each physical experiment (which are simulated by buoyancy surpluses or deficiencies). Such errors are a result of mass differences in in the PLA models and their counterweights, causing deviation from the target buoyancy values.

Orname ntation	Thrust Capability	Direction	PLA Model	Counter weight	Model Buoyancy	Target Buoyancy	Error (%)
			Mass (g)	Mass (g)	(dyn)	(dyn)	
Yes	Nautilus-Like	Upwards	132.91	2.4	1089	1047	4.01
Yes	Coleoid-Like	Upwards	130.54	4.05	2930	2670	9.74
No	Nautilus-Like	Upwards	136.35	0.72	1088	1047	3.92
No	Coleoid-Like	Upwards	130.01	7.11	2820	2670	5.62
Yes	Nautilus-Like	Downwards	132.91	4.60	-1069	-1047	2.10
Yes	Coleoid-Like	Downwards	132.91	7.06	-2540	-2670	-4.87
No	Nautilus-Like	Downwards	136.35	2.86	-1010	-1047	-3.53

No	Coleoid-Like	Downwards	136.35	6.41	-2670	-2670	Below
							Detection
Yes	N/A	Neutral	130.54	7.02	20	0	Below
		Rotation					Detection





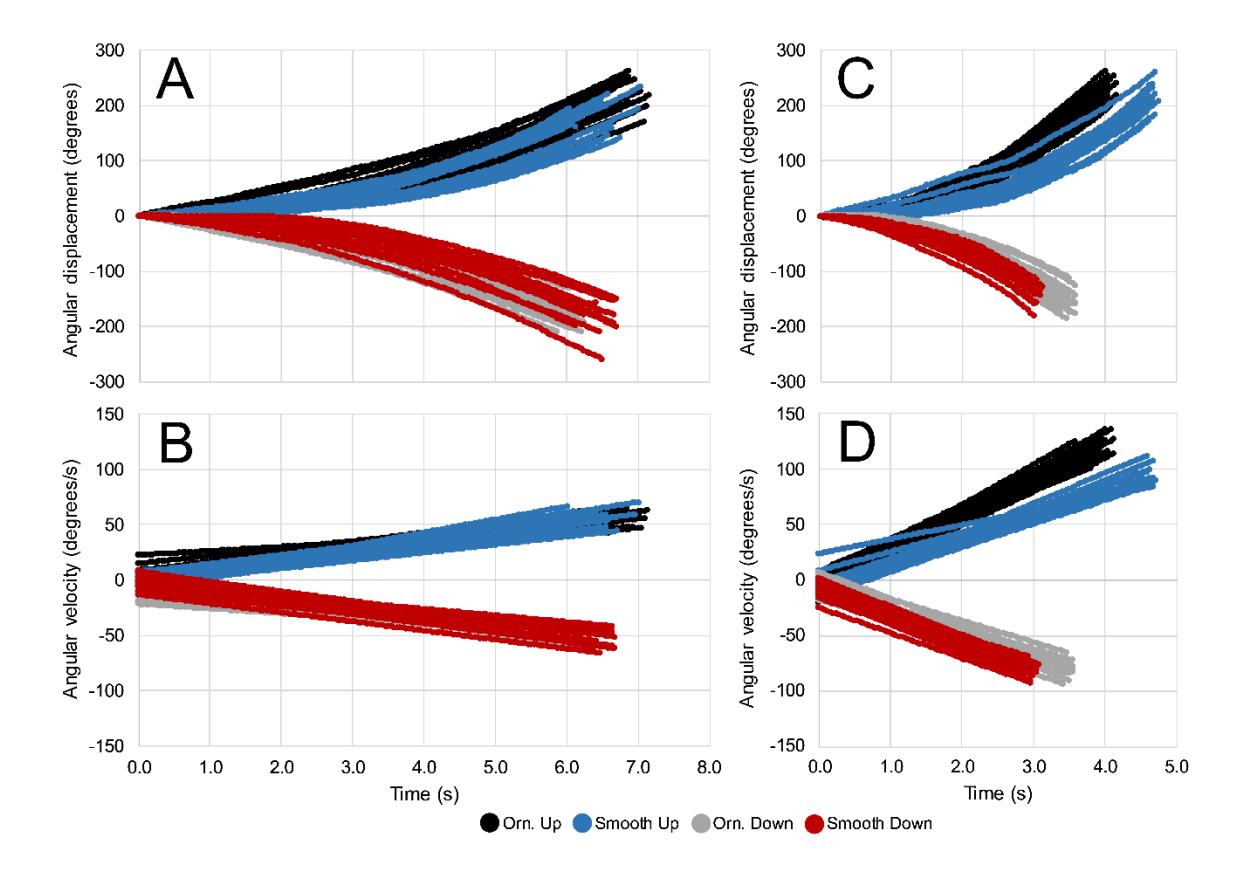


Figure 8: Motion tracking results of the vertical motion experiments on the ornamented and smooth physical models. A) Angular displacement (in degrees) from the starting position and B) angular velocities (degrees/s) for models with *Nautilus*-like thrusts. B) Angular displacement (in degrees) from the starting position and D) angular velocities (degrees/s) for models with coleoid-like thrusts. Positive values denote aperture-backwards rotation, which occurred during upward movement. Negative values denote aperture-forwards rotation, which occurred during downward movement.

Physical Experimentation on Neutrally Buoyant Models

 After pushing the neutrally buoyant model at various initial angular velocities (Table 5), their angular velocities decrease rapidly, then begin to asymptotically approach zero (Fig. 9A). The magnitude of torque also

decreases in this fashion (Fig. 9B). Angular velocities corresponding to torques less than or equal to the estimate of gill ventilation (13.2 dyn·cm; Fig. 9C) suggest that this small thrust can sustain angular velocities of 17 to 22 degrees per second (Fig. 9D). However, acceleration from a stationary initial condition was not considered here.

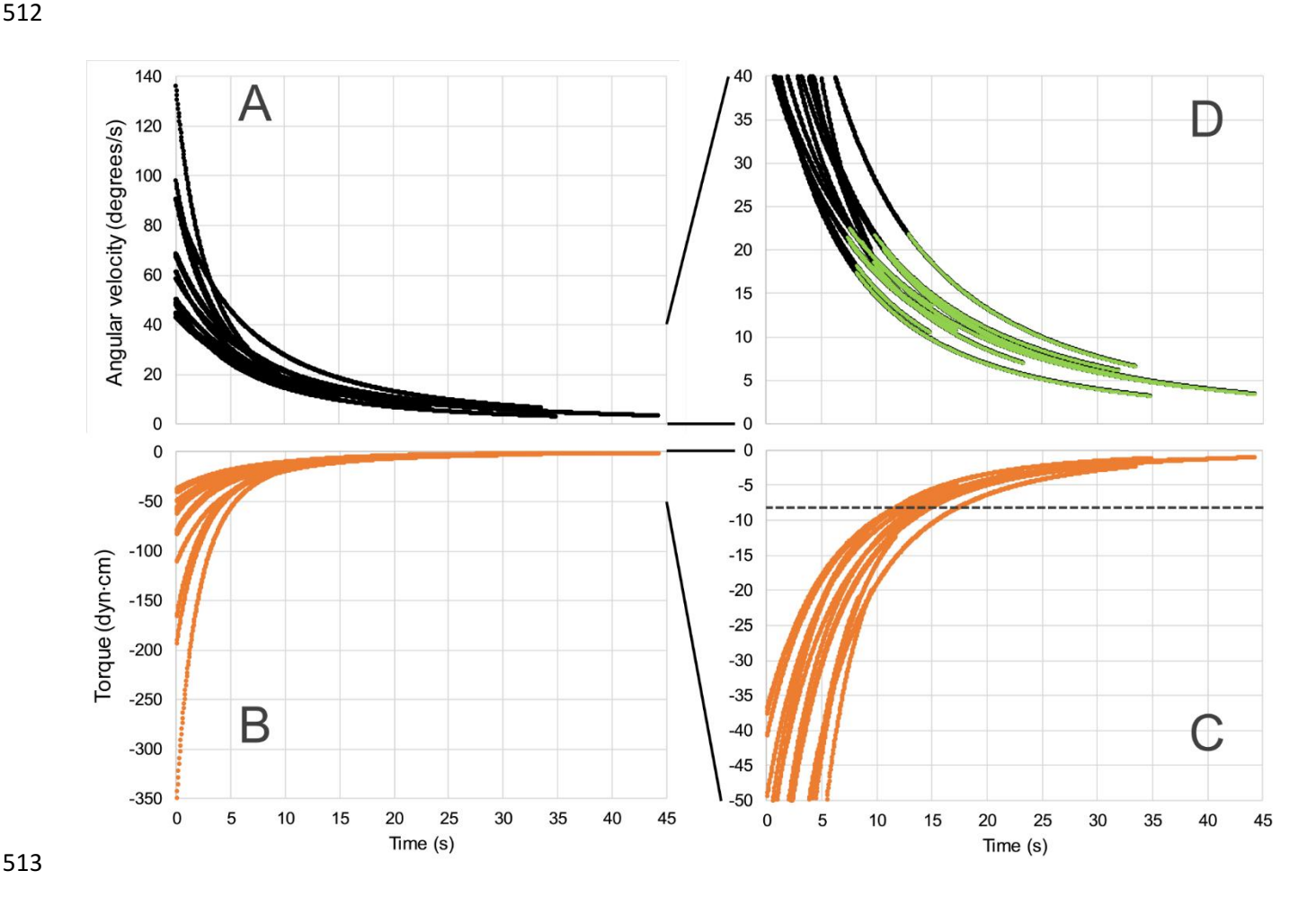


Figure 9: Motion tracking results of the neutrally buoyant *Mariella brazoensis* model. A) Angular velocities of 15 trials where the model was pushed at differing initial angular velocities. Afterwards hydrodynamic drag was responsible for decelerating the model. B) Torques occurring on the model in response to interaction with the surrounding fluid. C) Close up of torque values with dashed line representing the torques produced at the hyponome during ventilation of the gills (13.2 dyn·cm). D) Close up of angular velocities. Light green points correspond to thrusts produced by ventilation of the gills, suggesting that angular velocities of around 17 to 22 degrees per second could be sustained with this metabolically inexpensive process.

521

522 523 r 524 H 525 r 526 t 527 i 528 H 529 y 530 v

532

531

533

534 535

536

The moment of inertia of the 3D printed torticone model (4.35*10⁻⁵ Kg*m²) varies from the virtual model (and the actual living animal) due to the complex geometries and non-uniform densities of the latter. Even though both the virtual and physical models have the same theoretical centers of mass and buoyancy, their masses surrounding the axis of rotation are distributed differently, which influences rotational resistance. The total moment of inertia of the virtual model with multiple components of different densities (4.65*10⁻⁵ Kg*m²) is only 6.55% greater, suggesting that the reduction of torque on the living animal would be negligibly different. Furthermore, modeling the torticone as a simple point mass at the hyponome revolving about the rotational axis yields an even larger moment of inertia (5.43*10⁻⁵ Kg*m²), but would only decrease the sustained angular velocity by a few degrees per second. Such differences could be more severe at higher modeled torques and angular velocities, however.

Table 5: Initial angular velocities (ω ; degrees per second) for each trial of the neutrally buoyant rotation experiment. R² values and coefficients are reported for the regression lines of angular displacement following Equation 4; (a*t)/(1+b*t). These coefficients were used to fit the angular displacement values recorded from each trial. The corresponding equations were later differentiated to compute angular velocity and angular acceleration.

Trial	Coefficient	Coefficient	r-	Initial
	a	b	square	ω
1	97.94	0.1294	0.9981	97.94
2	136.20	0.1688	0.9984	136.2
3	61.60	0.0840	0.9992	61.6
4	48.15	0.0764	0.9991	48.15
5	58.79	0.0654	0.9986	58.79
6	44.31	0.0603	0.9995	44.31
7	90.89	0.1196	0.9996	90.89
8	68.49	0.0795	0.9992	68.49
9	68.95	0.0782	0.9992	68.95
10	49.15	0.0831	0.9994	49.15
11	67.52	0.0778	0.9999	67.52
12	44.73	0.0541	0.9996	44.72
13	43.25	0.0570	0.9996	43.25

Ī	14	90.56	0.0804	0.9972	90.56
	15	50.58	0.0640	0.9984	50.58

DISCUSSION

537

538

539

540

541

542

543

544

545

546

547

548

549

550

551

552

553

554

555

556

557

558

559

The Hydrostatic Properties of Torticone Cephalopods

Our results suggest that Mariella brazoensis, and torticones with similar proportions, had the capacity for neutral buoyancy, and were not restricted to the seafloor. A small amount of surplus cameral liquid could have been retained to produce slightly negative buoyancy, which would have been easier to manage compared to perfectly-neutral or positively-buoyant conditions (Ward and Martin, 1978; Ward, 1979a). In our shell model analyses, body chamber lengths of 1.5 whorls result in positive buoyancy, and still require some cameral liquid to remain in the chambers. With a larger body chamber length of around two whorls (body chamber length 50% of the total curvilinear length), the model becomes negatively buoyant with about 2.7% of the organismal mass not relieved by buoyancy. While larger body chamber ratios (by number of whorls) have been reported for some torticones (Klinger, 1981), it is not likely that they strongly exceed 40% of the total curvilinear length. Highspired torticones with low rates of whorl expansion could have maintained such body chamber lengths, while occupying more whorls. Some nautiloid torticones (e.g. some Brevicoceratidae, like Foersteoceras; Teichert et al., 1964) have densely packed septa in addition to large body chambers. Such morphologies may have struggled to attain near neutral buoyancy. For turrilitids, the limited oxygen isotope data (Henderson and Price, 2012) suggests that these ammonoids inhabited bottom to midwater depths. This range of depths agree with the buoyancy simulations in the current study since they were not strictly confined to the seafloor, despite their ostensible convergence upon gastropods (Berry, 1928; Ebel, 1992; Wiedmann, 1973).

Substantial amounts of cameral liquid could not be retained for neutral buoyancy. In turrilitids, the migration of the siphuncle to the mid- to upper flanks of the outer whorls has been interpreted as an adaptation to decouple cameral liquid (Ward, 1979a; Klinger, 1981). If cameral liquid remained in every chamber after becoming decoupled (losing direct contact with the siphuncle), the living torticone would be negatively

buoyant. However, the capillary membrane (pellicle) lining the camerae would have facilitated cameral liquid transport even if liquid was not in direct contact with the siphuncle (Denton and Gilpin-Brown, 1966; Weitschat and Bandel, 1991; Hoffmann et al., 2015). Furthermore, this siphuncle position may not substantially limit osmotic pumping at different depths (Diamond and Bossert, 1968; Greenwald et al., 1982; Jacobs, 1996; Hoffmann et al., 2015). If the siphuncle position just slowed cameral liquid transport (Ward, 1979a), perhaps more liquid was retained only in the adoral-most camerae, so that buoyancy was not adversely reduced. It is possible that an apical siphuncle position allowed quicker, minute changes in buoyancy because modifying the osmolarity of the entire decoupled liquid volume may not have been necessary (Denton and Gilpin-Brown, 1973: Ward and Martin, 1978: Ward, 1979b). The retention of cameral liquid in the corrugated septal margins (i.e., Peterman and Barton, 2019) may have served as liquid reserves to allow a greater range of buoyancy changes for vertical migration or faster refilling (Daniel et al., 1997). Extant Nautilus primarily achieve vertical migration with active jet propulsion, rather than passive buovancy changes (Ward, 1979b). The hyponomic sinuses of some torticones support a similar active locomotion strategy for these species. Perhaps turrilitids were capable of using both strategies to change their position in the water column, or each strategy depended upon the morphological capabilities of a particular taxon. If an adaptive function of the siphuncle position in turrilitids exists, it remains enigmatic and warrants further study, but does not reject our hydrostatic interpretations of M. brazoensis and similar ammonoids as free-living open-water animals.

560

561

562

563

564

565

566

567

568

569

570

571

572

573

574

575

576

577

578

579

580

581

582

583

Hydrostatic stability in *Mariella brazoensis* is greater than that of living *Nautilus* (0.05; Peterman et al., 2019) and is similar to that of other adult heteromorphs that separate their body chamber from their phragmocone (Peterman et al., 2020a, 2020b, 2020c). The key influence on mass distribution in cephalopods is held by the soft body – it's extent, position, and composition. Positioning the entire soft body beneath the phragmocone is the optimal way to increase hydrostatic stability. Hydrostatic stability would further increase as the apical angle decreases (e.g. *Turrilites costatus*) and as the shell uncoils (e.g. the nostoceratid, *Hyphantoceras orientale*). Orthocone cephalopods serve as the endmember of this highly stable strategy

(Peterman et al., 2019). As suggested by Ward (1979a), torticones are more stable than planispiral ectocochleates with similar whorl expansion rates. The current hydrostatic simulations suggest that the orientation of torticone cephalopods was somewhat fixed, and could not be substantially modified through active jet propulsion, or through the influence of external forms of energy (e.g., wave action and predator wake).

The shell is oriented apex-upwards, with the coiling axis displaced by about 8° from the vertical (Fig. 3A). The soft body is almost horizontally facing and tilted slightly upwards (12.3°; Fig. 3A; Table 2). This orientation depends on the obliquity of the shell's ornamentation, which denotes former positions of the aperture throughout ontogeny. Rib obliquity varies between species of turrilitids, but aligns with the current results. Depending on the morphology of the soft body and the size of the protruding arms, the benthos could have been accessed with this orientation. A horizontally-facing orientation would have also enabled feeding within the water column. Perhaps one or both of these strategies were used, depending on the taxon.

Our hydrostatic model and hydrodynamic simulations show that lateral motion would be inefficient in torticone ammonoids (Figs. 3 and 7; Tables 2 and 3). Much of the energy produced by jet propulsion would be lost to rocking due to the low position of the hyponome relative to the horizontal rotational axis (Fig. 3 A and C). This low thrust angle ($\theta_t = -74.1^{\circ}$) would be much better suited for upwards vertical movement if the hyponome was able to bend in the antapical direction. The ability for locomotion in this direction is reinforced by the well-developed hyponomic sinuses of some turrilitid species (Klinger, 1981). Indeed, vertical movement potential of torticones has been ranked higher relative to their horizontal movement potential (Klinger, 1981; Westermann, 1996; Naglik et al., 2015a). Our computational fluid dynamics simulations also support vertical locomotion; hydrodynamic drag is lower in the vertical directions (up or down) than the horizontal direction (i.e., moving laterally away from the aperture; Fig. 7; Table 3). Using a water jet to create horizontal movement would require the ammonoid to bend its hyponome at a 90° angle to direct thrust away from, or toward, its vertical rotational axis, which aligns to the centers of buoyancy and of mass. Even in this case, the low thrust

angle would cause much energy to be lost to rocking. For almost any other hyponomic orientation, rotation about the vertical axis would likely occur. Their poor horizontal movement potential suggests that turrilitids were dispersed to their wide biogeographic distributions by currents during their planktic, juvenile stages (Landman et al., 1996).

Our results support and refine rotation motions predicted in torticone ammonoids. Previous observers (Ward, 1979a; Klinger, 1981) suggested that spinning would be a natural consequence of locomotion in torticone shells. Adding constraints to this interpretation, our hydrostatic results reveal that the hyponome would only have to bend about 20° from the direction the aperture is facing (from 110.1° to 90°) to most-efficiently transmit thrust into rotation. Energy would still be lost, however, due to the low position of the hyponome relative to the centers of buoyancy and mass, yielding both wobble and precession about the vertical rotational axis. Torticones with larger lever arms (lower apical angles) may have increased torque for better rotation about this vertical axis. However, torticones with low apical angles would have had more mass concentrated towards their rotational axis, lowering their moments of inertia. This mass distribution may have compensated for the reduction of the lever arm, allowing similar angular accelerations in response to different torques. The relationship between these two quantities is complex and should be studied further. These hydrostatic properties strongly constrain the movement of torticone cephalopods since thrust in almost any horizontal direction would result in some amount of rotation.

Passive Rotation During the Vertical Movement of Torticones

The results of our physical experiments show that rotation occurs easily with any vertical motion of the shell – up or down – in the water column. For these first-order experiments, we 3D printed shell models with negative, neutral, and positive buoyancy commensurate with propulsive abilities we might estimate for the ammonoid animal. While downward movement was likely a result of slight negative buoyancy rather than active locomotion, its force was held the same as the other directions to compare between experiments. Due to the lack of ammonoid soft body preservation in the fossil record (Klug et al., 2012; Klug and Lehmann, 2015),

the propulsive abilities of other cephalopods must be used as analogues (Jacobs and Landman, 1993). The *Nautilus* likely serves as a reasonable analogue for the available thrust produced by torticones (when scaled by mass). This estimate may be conservative, considering the closer phylogenetic position of ammonoids to coleoids (Kröger et al., 2011; Klug et al., 2015), which are generally more active. In contrast, the *Nautilus*-like estimates may be preferred due to the low metabolism inferred for some torticones (Henderson and Price, 2012). Vertical movement of 3D printed models result in rotation about the vertical axis with both *Nautilus*-like and coleoid-like thrusts. Adding to the experimental observations, we simulated flow around the shell using computational fluid dynamics (CFD), which reveal incident streamlines rotating about stationary models (Figs. 5 and 6). In the upward direction the simulations illustrate flow remarkably similar to the rotational trajectories in our experiments (angular displacement; Fig. 8A and B). Downward movement is more complicated, but pressure gradients on the underside of the shell suggest that aperture forward rotation is a result of the incident fluid first encountering the antapical part of the first whorl, in addition to lower pressure zones around the aperture and along the shell flanks. Altogether, the expectation for passive rotation during vertical movement is well constrained.

Ecological Interpretations

The 3D printed models rotate aperture-backwards during upward movement (Figs. 8 and 10A). Passive twirling could allow a torticone ammonoid to forage and grasp for plankton through a broader sweep of the water column as it rose or fell. Hyponomic sinuses present on several torticones (e.g. *Turrilites costatus* Lamarck, 1801; *T. scheuchzerianus* Bosc, 1801) suggests that the downwards production of thrust was regularly involved for upwards vertical movement (Klinger, 1981), perhaps as vertical escape tactics if acceleration was sufficient. Because torticone ammonoids were diverse and disparate, some morphologies may have been favorable for vertical movement, while others favored demersal habits. Torticones with low apical angles (e.g. many *Turrilites*, *Mariella*, and *Ostlingoceras*) were likely better-suited for vertical movement than morphologies with wide apical angles (e.g. several species of *Hypoturrilites*; Klinger, 1981; Westermann,

1996). Perhaps, demersal torticones behaved as saltators – briefly rising from the seafloor while rotating, then scavenging or pouncing on benthic prey at a new location. Active hunting, however, would depend upon the field of view for these cephalopods, which may have been limited during rotation.

Due to the obstruction of the hyponome by the overlying shell and soft body, it is unlikely that downwards movement would occur via jet propulsion. A more likely scenario for movement in the downwards direction involves sinking due to slight negative buoyancy. This condition could be attained by simply retaining a few grams of excess cameral liquid in the phragmocone. It was likely easier to manage this slightly negative buoyancy rather than positive buoyancy, especially considering the upwards obstruction of the hyponome.

Similarly, extant *Nautilus* are reported to be slightly negatively buoyant (<1% of organismal mass not relieved by buoyancy; Ward and Martin, 1978; Ward, 1979a). During downwards movement, the 3D printed torticone models rotate aperture-forward (Figs. 8 and 10B). Perhaps this direction of movement was favorable for feeding on plankton in the water. Torticones that experienced vertical migration could have risen in the water column, and fed on the way down, taking advantage of the passive movement induced by shell shape during slow sinking.

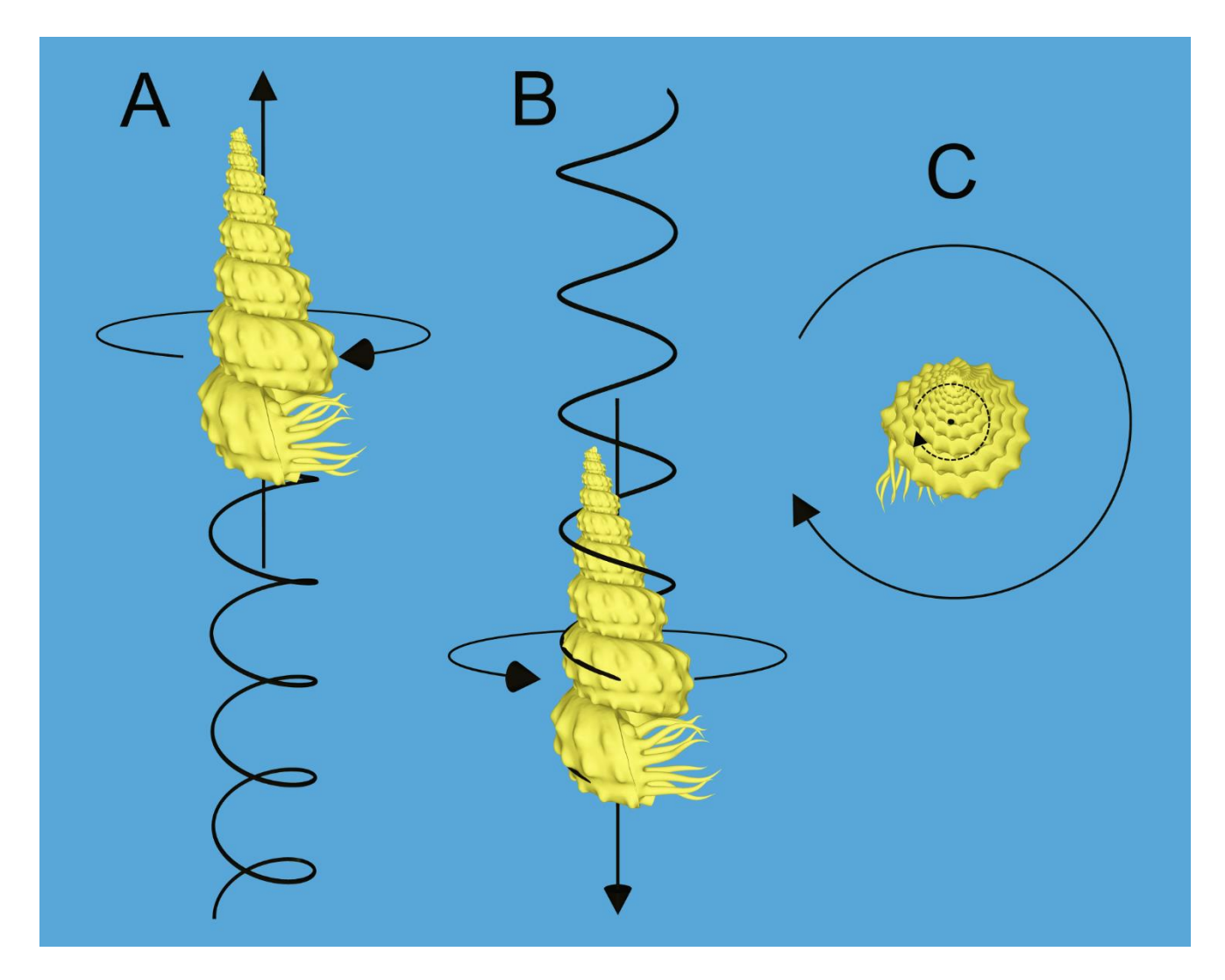


Figure 10: Depiction of movement directions during physical experiments. A) Upward movement resulting in consistent aperture-backwards rotation. B) Downward movement resulting in consistent aperture-forwards rotation. C) Depiction of the precession of the shell's coiling axis (dashed line showing path) about the vertical axis (black point in center).

Both proposed life habits are supported by the available data of oxygen isotopes for some turrilitid ammonoids. Henderson and Price (2012) reported oxygen isotope values that are consistent with the inhabitation of bottom to midwater depths for *Hypoturrilites gravesianus* (d'Orbigny, 1842) and *Turrilites costatus*. Variability in isotopic values within single specimens may be the result of vertical migration (in addition to seasonal variability). However, ontogenetic sampling of these ammonoids (e.g. Fatherree et al., 1998; Lukeneder et al., 2010) was not within the scope of their study.

The coiling axis undergoes precession about the vertical axis during rotation (Fig. 10C). Higher thrust values cause the apex to tilt more than its usual 8° during upwards movement. It is unlikely that the living animal was able to remediate this by changing its mass distribution. This tilt may pose an upper constraint on vertical velocity. Average vertical velocity values for each thrust scenario are approximately 8.5 to 12.0 cm/s. While the models accelerated in the vertical direction, they did not reach their maximum velocities due to the size limitations of the water tank (70 cm of vertical liquid). Experiments performed in a larger vertical column of water can elucidate the vertical velocity constraints in each direction. While instantaneous vertical velocity and acceleration could not be quantified, the models were slow to rise directly after being released. This behavior suggests that torticones may have not been able to perform in rapid vertical escape maneuvers, like those suggested for orthocones (Westermann, 1996).

There are no considerable differences in angular displacement or angular acceleration between the ornamented models resembling *Mariella brazoensis* and the theoretical, smooth models (Fig. 8). The error in mass (and therefore buoyancy; Table 4) between each of the 3D printed models accounted for minor differences in angular velocity during vertical movement for each experiment (Fig. 8C and D). This relationship suggests that the ornamentation does not enhance or diminish angular velocity (at the vertical velocities and thrusts experimented upon in the current study). If the tilted ornamentation served a hydrodynamic function, it may have performed stabilization during vertical movement (Ifrim, 2018). This function is suggested by the streamlines being directed in between tubercles (Fig. 5); however, the significance of this channeling is unknown since it was not quantified in any of the experiments. Future hydrodynamic experiments could be designed to investigate the stabilizing function of ornamentation during movement. Alternatively, the rib and tubercle obliquity on each whorl may be an artifact of the apertural orientation at any given point during life. Robust turrilitid ornamentation could have served another adaptive function – likely protection against predators. Some turrilitids had spines projecting from their tubercles (e.g. some species of *Mariella*; Matsumoto and Kawashita, 1999) and the presence of such spines are biased by the lack of aragonitic shell preservation

(especially within notable Cenomanian deposits worldwide; Kennedy and Cobban, 1976; Klinger and Kennedy, 1978; Kennedy et al., 2005). Some turrilitid spines were hollow, with septa at their bases that prevented the connection of these voids to the camerae (Klinger, 1981). Klinger (1981) speculated on the hydrostatic influences of these fluid-filled, hollow spines. While they would have indeed added more mass to the living turrilitids, they also protected them from suffering a decrease in buoyancy in the event of a broken spine, which would cause their chambers to fill with seawater. Such a scenario was likely fatal, causing immobilization or sinking to the sea bottom. Septate spines are also consistent with non-benthic life habits for these torticones since they have built-in countermeasures to prevent substantial negative buoyancy. Alternatively, these forms of ornamentation could have been used for sensory purposes (Ifrim et al., 2018).

If rotational movement was not preferred by the living cephalopod (momentarily or generally), aperture-forwards movement could have been simply counteracted via jetting from the hyponome. At the higher timesteps, the model experiences a net torque of around 5,400 dyn·cm in the aperture-forward direction.

Coleoid-like jetting torque is almost equal to this value, and *Nautilus*-like torque is about half. Therefore, it should only take a few pulses of jet thrust to disrupt rotation. The torque produced by ventilation is several orders of magnitude lower, suggesting that its influence is minimal. Aperture-backwards movement would be harder to counteract, because the hyponome would have to bend beneath the shell in the opposite direction of the aperture (>90°). This may have been easier for torticones with hyponomic sinuses. Depending on the soft body morphology, the arrangement of the arms may have allowed the living cephalopod to manipulate its hydrodynamic drag, slowing rotation. It is feasible that torticones were able to enhance or diminish passive rotation induced by vertical movement depending upon their desired life habits.

Sustaining slow rotation with minimal effort

Physical experiments on a neutrally buoyant model demonstrate that slow rotation requires low amounts of torque to sustain (Fig. 9). For the modeled *Mariella brazoensis*, an estimate of the small thrusts produced during the regular ventilation of its gills, would have produced torques that could sustain angular velocities of

approximately 17 to 22 degrees per second (Fig. 9D). Therefore, while simply "breathing" and pointing the hyponome normal to the lever arm, it would take around 16 to 21 seconds to complete one revolution. While we did not investigate acceleration from a stationary initial condition, these results suggest that it would take minimal effort to sustain movement once active locomotion is used to start spinning. The metabolic cost of such a behavior would be low, which conforms with the limited carbon isotope data for turrilitids (Henderson and Price, 2012). More-rapid turns could have taken place during normal jet thrusts since the torques produced would have been more than five times higher than those observed in the experiments. This relationship is complicated however, because of the nonlinear deceleration of the model in response to hydrodynamic drag. More experiments at higher torques can be performed, but an adaptive advantage of high velocity spinning seems unlikely. While spinning would not be useful to avoid predation from large, shell crushing predators, smaller predators (crustaceans, small fish, and other cephalopods) may have had access to the soft body denied after a quick 180° rotation. Spinning about the vertical axis would have allowed the living cephalopod to move at low metabolic cost. The poor horizontal mobility of these cephalopods suggests that they assumed sluggish life habits, while exploiting vertical directions to search for small prey.

Boom and bust for Cretaceous Turrilitids

Our results suggest that *M. brazoensis* could forage for planktic prey items while exerting little energy. None of our results suggest that these animals were active hunters through sustained, directed propulsion; nor would we expect brief intervals of rapid escape. With simple propulsion yielding an easy survey of their feeding grounds, these animals could operate on low metabolic demands. In turn, we would interpret that they functioned as mid-tier holozooplankton, producing meals for larger ammonoids (during their planktic, juvenile stages) or for vertebrate predators. High fecundity would fit with their distribution, abundance, and rapid diversification (Landman et al., 1996); moreover, low metabolic demands and high fecundity would help explain their hydrodynamic disadvantages for actively chasing prey or dodging their predators. The cosmopolitan distribution of several turrilitid genera in the Cenomanian (Kennedy and Cobban, 1976; Wright et

al., 1996; Page, 1996; Ifrim et al., 2015) should certainly relate to passive distribution (particularly of juveniles) along oceanic currents. Similarly, relatively passive distribution along fragmenting neritic and epicontinental seas could easily allow their diversification via endemism in the interval of rising sea levels (Hancock and Kauffman, 1979; Hay, 2008; Olde et al., 2015) and the simultaneous dispersal of cosmopolitan taxa (Yacobucci, 2017). In warm neritic seas (Caldeira and Rampino, 1991; Jenkyns et al., 1994; Huber et al., 2002) with high productivity fed by heightened terrigenous runoff and expanding euphotic habitats, conditions were optimal for torticone-shelled ammonoids, feeding near the seafloor or within the water column. However, life at the margins has its limits and environmental or ecological conditions culminating in the Ocean Anoxic Event (OAE2) were less supportive of the passive, planktivorous, high-fecundity life habit that had previously served the torticones so well.

Coupling this interpretation of our test subject with Yacobucci's (2017) finding that the C-T crisis did not substantially elevate global ammonite extinction rates yields predictions for the ecology of ammonoids that survived into the Turonian, and later diversified. The turrilitid torticones once flourished within a middling trophic rank, feeding with low metabolic cost. After this extinction, helical coiling and its accompanying hydrodynamic constraints appeared in a small number of heteromorphs, mostly occurring within a fraction of their subadult ontogeny. The considerable reduction of this once-successful life habit suggests that the ecological challenges changed for ammonoids heading into the C-T transition, even if it did not produce a global mass extinction among ammonoid species. Environmental shifts could have triggered any variety of escalations: competition for prey; ambition of predators. Population dips that hindered fecundity in critical generations or regions, could easily derail a species, or larger clade, that relied on numbers of individuals to compensate for their lack of defensive strategies.

Morphological changes in ammonoids crossing the Cenomanian-Turonian boundary yield testable predictions. Ammonite clades that flourished (via diversity, abundance, size, or distribution) leading into the early Turonian should have shells that are better-suited to interspecies cephalopod competition. In the

hydrodynamics sense, this should include shells that allowed faster swimming, even for brief intervals to dodge a predator; and/or shells that were more efficient in lateral propulsion. This should include planispiral shells for lateral movements and orthoconic shells for vertical movement. In the hydrostatic sense, this should include species whose shells provided stability both at rest and in motion. Shells with greater spatial distinction of their body chamber and buoyant phragmocone (i.e., scaphitids), and/or with higher whorl expansion rates, would meet these criteria. Regarding biomineralization, the successful early Turonian species should produce shells with greater material efficiency, or prioritized size acquisition. Planispiral shapes can house more body with less material by accreting closely to the previously-occupied body chamber. High whorl expansion rates and compressed thickness ratios can produce a large diameter shell, which, viewed from the side by a prospective predator, can look larger than a shell with the same biomineralized material in a sphaerocone or planorbicone shape. These hypotheses can readily be tested with additional comparison of morphotype expression in species across the C-T transition, and additional analysis of species' hydrostatics and hydrodynamics via experiments and simulations. Overall, perhaps ammonoids weathered the OAE2 (and preceding environmental changes) with their classic boom-and-bust plasticity in form and diversification: removing twirling torticones in favor of faster forms.

CONCLUSIONS

777

778

779

780

781

782

783

784

785

786

787

788

789

790

791

792

793

794

795

796

797

798

799

800

Torticones with similar proportions to the modeled turrilitid, *Mariella brazoensis*, were capable of neutral buoyancy, which rejects gastropod-like analogies for their life habit. This morphotype was hydrostatically stable, and the horizontally-facing soft body orientation could not be considerably modified with active locomotion or surrounding water currents. Depending on the soft body morphology, this orientation could have allowed feeding on the seafloor, or within the water column. Thrust angles reveal that horizontal locomotion would result in substantial energy loss due to rocking. The source of thrust is better aligned with the centers of buoyancy and mass in the vertical direction, suggesting that upwards vertical movement would be

much more efficient. This movement direction is also supported by CFD simulations, which reveal that hydrodynamic drag is lower in the vertical directions compared to horizontal movement. The rotational thrust angle suggests that thrust in almost any feasible hyponome orientation (especially within the horizontal plane) would result in energy transmitted into rotation about the vertical axis.

Computational fluid dynamics simulations reveal that the corkscrew shape of the shell would interact with incident flow in such a way that could produce rotation about the vertical axis during vertical movement. Physical models, 3D printed to simulate artificial thrusts via buoyancy adjustments, confirm that passive rotation occurs at significant angular velocities. Upward movement results in aperture-backward rotation, while downward movement results in aperture-forward rotation. These forms of rotation may have been useful during vertical migration to search for planktic prey, or to detect potential predators. Ornamentation of the shell does not seem to influence rotation magnitude during movement even though the tubercles and ribs on many torticones are consistently tilted. This indifference suggests that ornamentation served another adaptive function; pertaining to other hydrodynamic properties (stabilization) or as a defense against predators. Neutrally buoyant models reveal that low thrusts/torques can sustain slow rotational movement. An estimate of the force produced by gill ventilation (involved in respiration) yields angular velocities of 17 to 22 degrees per second. Thus, rotation about the vertical axis would have required little energy.

While torticones were somewhat morphologically disparate, rotation was likely involved in most forms of movement, which would have strictly constrained their life habit and ecology. Rotational movement could have facilitated feeding within the water column, scavenging the benthos, expanding the field of view, or effortlessly turning to deny soft body access to small predators. Sluggish life habits are inferred for these cephalopods which utilize metabolically inexpensive rotation occurring from both active locomotion and passively from vertical migration in the water column. These life habits would have been well suited for planktivory, suggesting that turrilitids would have been susceptible to the decline or turnover in such food sources approaching the Cenomanian-Turonian extinction.

Q	2	5	
u	_	J	

ACKNOWLEDGEMENTS

- We appreciate the help of K. Hollis, H. Little, and M. Florence (Smithsonian National Museum of Natural History) for their help with specimen USNM 430965, which was used in photogrammetry. We also
- thank R. Lemanis, P. Ward, and J. Slattery for constructive reviews that improved the quality of the paper.
 - Finally, we thank the National Science Foundation for supporting this research (Award #1952756).

831

832

833

835

836

830

REFERENCES

- 3DFLOW, 2018, 3DF Zephyr free edition. 3Dflow s.r.l., Verona, Italy.
- ANSYS Inc., 2019, ANSYS Fluent 2019 R2. ANSYS Inc., Canonsburg, Pennsylvania, USA.
 - ARTHUR, M.A., SCHLANGER, S.O., JENKYMS, H.C., 1987, The Cenomanian-Turonian oceanic anoxic
 - event II. Paleoceanographic controls on organic matter production and preservation, in BROOKS, J.,
- FLEET, A.J. (eds.), Marine petroleum source rocks: Geological Society of London Special Publication,
- v. 26, p. 401–420.
- ATABEKIAN, A.A., 1987, Turrilitidae de l'Albien supérieur et du Cénomanien du sud de l'URSS, Association
- Géologique Auboise, Ste Savine, France, 121 p.
- Autodesk Inc., 2017a, Meshmixer 3.3. Autodesk Inc., San Rafael, CA.
- Autodesk Inc., 2017b, Netfabb 2017.3. Autodesk Inc., San Rafael, CA.
- BATT, R.J., 1989, Ammonite shell morphotype distributions in the Western Interior Greenhorn Sea and some
- paleoecological implications: PALAIOS, v. 4, p. 32–42.
- BERRY, E.W., 1928, Cephalopod adaptations the record and its interpretation: Quarterly Review of Biology,
- v. 3, p. 92–108.
- Blender Online Community, 2017, Blender, a 3D modelling and rendering package. Blender Institute,
- Amsterdam. Available at: http://www.blender.org. Accessed 1 June 2018.

BOSC, L.A.G., 1801, An 13 *in* F. Roissy (ed.), Histoire naturelle générale et particulière, des mollusques, animaux sans vertebrés et a sang blanc. Ouvrage faisant suite aux Oeuvres de Leclerc de Buffon, et partie du Cours complet d'Histoire naturelle, rédigé par C.S. Sonnini, member de plusieurs Sociétés

savantes. Continué par F. de Roissy. Chez Deterville, Paris, 448 p.

852

856

857

858

859

860

861

862

863

864

865

866

867

868

869

- BRONGNIART, A. 1822, Sur quelques terrains de Craie hors du Bassin de Paris, *in* Cuvier, G., Brongniart, A. (eds.), Description géologique des environs de Paris, 3rd ed., 428 pp. Dufour & d'Ocagne, Paris, p. 80–101.
 - BROWN, D., 2017, Tracker 4.11.0. Available at: https://physlets.org/tracker/. Accessed 21 June 2018.
 - CALDEIRA, K., and RAMPINO, M.R., 1991. The mid-Cretaceous superplume, carbon dioxide, and global warming: Geophysical Research Letters, v. 18, p. 987–990.
 - CHAMBERLAIN, J.A., 1990, Jet propulsion of *Nautilus*: a surviving example of early Paleozoic cephalopod locomotor design: Canadian Journal of Zoology, v. 68, p. 806–814.
 - CIGNONI, P. and RANZUGLIA, G., 2014, MeshLab. Version 1.3.3. Visual Computing Lab, Pisa, Italy.

 Available from: http://meshlab.sourceforge.net/. Accessed 1 August 2018.
 - COBBAN, W.A., 1971, New and little-known ammonites from the Upper Cretaceous (Cenomanian and Turonian) of the Western Interior of the United States: Geological Survey Professional Paper 699, 61 p.
 - COBBAN, W.A., HOOK, S.C., and McKINNEY, K.C., 2008, Upper Cretaceous molluscan record along a transect from Virden, New Mexico, to Del Rio, Texas: New Mexico Geology, v. 30, p. 75–92.
 - DANIEL, T.L., HELMUTH, B.S., SAUNDERS, W.B., and WARD, P.D., 1997, Septal complexity in ammonoid cephalopods increased mechanical risk and limited depth: Paleobiology, v. 23, p. 470–481.
 - DENTON, E.J., and GILPIN-BROWN, J.B., 1966, On the buoyancy of the pearly *Nautilus*: Journal of the Marine Biological Association of the United Kingdom, v. 46, p. 723–759.
- DENTON, E.J., and GILPIN-BROWN, J.B., 1973, Flotation mechanisms in modern and fossil cephalopods:

 Advances in Marine Biology, v. 11, p. 197–268.

- DIAMOND, J.M., and BOSSERT, W.H., 1968, Functional consequences of ultrastructural geometry in
- "backwards" fluid-transporting epithelia: The Journal of Cell Biology, v. 37, p. 694–702.
- DIETL, G., 1973, Middle Jurassic (Dogger) heteromorph ammonites, in Hallam, A. (ed.), Atlas of
- Paleobiogeography: Elsevier, Amsterdam, p. 283–285.
- D'ORBIGNY, A.D., 1842, Paléontologie française: Terrains crétacés. 1. Céphalopodes. Masson, Paris, p. 431–
- 878 662.

886

- DRUSHCHITS, V.V., DOGUZHAEVA, and MIKHAILOVA, I.A., 1977, The structure of the ammonitella and
- the direct development of ammonites: Paleontological Journal, 1977, no. 2, p. 188–199.
- EBEL, K., 1992, Mode of life and soft body shape of heteromorph ammonites: Lethaia, v. 25, p. 179–193.
- 882 ELDER, W.P., 1989, Molluscan extinction patterns across the Cenomanian–Turonian boundary in the western
- interior of the United States: Paleobiology, v. 15, p. 299–320.
- 884 ELDERBAK, K., LECKIE, R.M., and TIBERT, N.E., 2014, Paleoenvironmental and paleoceanographic
 - changes across the Cenomanian-Turonian Boundary Event (Oceanic Anoxic Event 2) as indicated by
 - foraminiferal assemblages from the eastern margin of the Cretaceous Western Interior Sea:
- Palaeogeography, Palaeoclimatology, Palaeoecology, v. 413, p. 29–48.
- FATHERREE, J.W., HARRIES, P.J., and QUINN, T.M., 1998, Oxygen and carbon isotopic "dissection" of
 - Baculites compressus (Molluscan: Cephalopodan) from the Pierre Shale (upper Campanian) of South
- Dakota: Implications for paleoenvironmental reconstructions: PALAIOS, v. 13, p. 376–385.
- 61 GIRAUD, F., REBOULET, S., DECONINCK, J.F., MARTINEZ, M., CARPENTIER, A., and BREZIAT, C.,
- 892 2013, The Mid-Cenomanian Event in southeastern France: evidence from palaeontological and clay
- mineralogical data: Cretaceous Research, v. 46, p. 43–58.
- 6894 GREENWALD, L., COOK, C., and WARD, P.D., 1982, The structure of the chambered *Nautilus* siphuncle: the
- siphuncular epithelium: Journal of Morphology, v. 172, p. 101–110.

- 686 GREENWALD, L. and WARD, P.D. 1987. Buoyancy in Nautilus. In: B.W. Saunders and N.H. Landman (eds.),
- Nautilus—The Biology and Paleobiology of a Living Fossil, Springer, Dordrecht, p. 547–559.
- HANCOCK, J.M., and KAUFFMAN, E.G., 1979, The great transgressions of the Late Cretaceous: Journal of
- the Geological Society, London, v. 136, p. 175–186.
- 900 HARRIES, P.J., 1993, Dynamics of survival following the Cenomanian-Turonian (Upper Cretaceous) mass
- extinction event: Cretaceous Research, v. 14, p. 563–583.
- 902 HARRIES, P.J., and LITTLE, C.T.S., 1999, The early Toarcian (Early Jurassic) and the Cenomanian-Turonian
- 903 (Late Cretaceous) mass extinctions: similarities and contrasts: Palaeogeography, Palaeoclimatology,
- Palaeoecology, v. 154, p. 39–66.
- 905 HAY, W.W., 2008, Evolving ideas about the Cretaceous climate and ocean circulation: Cretaceous Research, v.
- 906 29, p. 725–753.
- 907 HEBDON, N., RITTERBUSH, K.A., and CHOI, Y., 2020a, Computational fluid dynamics modeling of fossil
- ammonoid shells: Palaeontologia Electronica, v. 23, a21, doi: 10.26879/956.
- 909 HEBDON, N., RITTERBUSH, K.A., and CHOI, Y., 2020b, Assessing the morphological impacts of ammonoid
- shell shape through systematic shape variation: Integrative and Comparative Biology, icaa067, doi:
- 911 10.1093/icb/icaa067.
- 912 HENDERSON, R.A., and PRICE, G.D., 2012, Paleoenvironment and paleoecology inferred from oxygen and
- carbon isotopes of subtropical mollusks from the Late Cretaceous (Cenomanian) of Bathurst Island,
- 914 Australia: PALAIOS, v. 27, p. 617–626, doi: 10.2110/palo.2011.p11-120r.
- 915 HIRANO, H., TOSHIMITSU, S., MATSUMOTO, T., and TAKAHASHI, K., 2000, Changes in Cretaceous
- ammonoid diversity and marine environments of the Japanese Islands, *in* OKADA, H., and MATEER,
- 917 N.J. (eds.), Cretaceous Environments of Asia, Elsevier, Amsterdam. P. 145–154.
- HOFFMANN, R. and ZACHOW, S., 2011, Non-invasive approach to shed new light on the buoyancy business
- of chambered cephalopods (Mollusca). In: *IAMG*, *Salzburg*, 2011, pp. 1–9.

- 920 HOFFMANN, R., SCHULTZ, J.A., SCHELLHORN, R, RYBACKI, E., KEUPP, GERDEN, S.R., LEMANIS,
- R., and ZACHOW, S., 2014, Non-invasive imaging methods applied to neo- and paleo-ontological
- cephalopod research: Biogeosciences, v. 11, p. 2721–2739.
- HOFFMANN, R., LEMANIS, R., NAGLIK, C. and KLUG, C. 2015. Ammonoid buoyancy, in Klug, C., Korn,
- D., De Baets, K., Kruta, I., and Mapes, R.H. (eds.), Ammonoid paleobiology. Vol. 1: from anatomy to
- ecology: Topics in Geobiology, 43. Springer, Dordrecht, The Netherlands, p. 611–648.
- 926 HOFFMANN, R., LEMANIS, R., FALKENBERG, J., SCHNEIDER, S., WESENDONK, H., and ZACHOW,
- 927 S., 2018, Integrating 2D and 3D shell morphology to disentangle the paleobiology of ammonoids: a
- virtual approach: Paleontology, v. 61, p. 89-104.
- 929 HUBER, B.T., NORRIS, R.D., and MACLEOD, K.G., 2002, Deep-sea paleotemperature record of extreme
- warmth during the Cretaceous: Geology, v. 30, p. 123–126.
- 1931 IFRIM, C., LEHMANN, J., and WARD, P., 2015, Paleobiogeography of Late Cretaceous ammonoids, in Klug,
 - C., Korn, D., De Baets, K., Kruta, I., and Mapes, R.H. (eds.), Ammonoid paleobiology. from
- macroevolution to paleogeography: Topics in Geobiology, 44. Springer, Dordrecht, The Netherlands, p.
- 934 515–538.

- 935 IFRIM, C., BENGTSON, P., and SCHWEIGERT, G., 2018, Growth and function of spines in Jurassic and
- Cretaceous ammonoids: Cretaceous Research, v. 88, p. 62–78.
- 937 INOUE, S., and KONDO, S., 2016, Suture pattern formation in ammonites and the unknown rear mantle
- 938 structure: Scientific Reports, v. 6, p. 33689.
- JACOBS, D.K., 1996, Chambered Cephalopod Shells, Buoyancy, Structure and Decoupling: History and Red
- 940 Herrings: PALAIOS, v. 11, p. 610–614.
- JACOBS, D.K. & LANDMAN, N.H. 1993. *Nautilus* a poor model for the function and behavior of
- 942 ammonoids?: Lethaia, v. 26, p. 1–12.

- JAGT-YAZYKOVA, E.A., 2011, Palaeobiogeographical and palaeobiological aspects of mid- and Late

 Cretaceous ammonite evolution and bio-events in the Russian Pacific: Scripta Geologica, v. 143, p. 15–
- 945 121.
- JAGT-YAZYKOVA, E.A., 2012, Ammonite faunal dynamics across bio-events during the mid- and Late

 Cretaceous along the Russian Pacific coast: Acta Palaeontologica Polonica, v. 57, p. 737–748.
- JENKYNS, H.C., 1980, Cretaceous anoxic events: from continents to oceans: Journal of the Geological Society,

 London, v. 137, p. 171–188.
- JENKYNS, H.C., GALE, A.S., and CORFIELD, R.M., 1994, Carbon- and oxygen-isotope stratigraphy of the
 English Chalk and the Italian Scaglia and its palaeoclimatic significance: Geological Magazine, v. 131,
 p. 1–34.
- JENKYNS, H.C., DICKSON, A.J., RUHL, M., and VAN DEN BOORN, S.H.J.M., 2017, Basalt-seawater
 interaction, the Plenus Cold Event, enhanced weathering and geochemical change: deconstructing
 Oceanic Anoxic Event 2 (Cenomanian–Turonian, Late Cretaceous): Sedimentology, v. 64, p. 16–43.
 - KAIHO, K., HASEGAWA, T., 1994, End-Cenomanian benthic foraminiferal extinctions and oceanic dysoxic events in the northwestern Pacific Ocean: Palaeogeography, Palaeoclimatology, Palaeoecology, v. 111, p. 29–43.
- KENNEDY, W.J., and COBBAN, W.A., 1976, Aspects of ammonite biology biogeography, and biostratigraphy: Special Papers in Palaeontology NO. 17, 94 p.
- KENNEDY, W.J., and COBBAN, W.A., 1990, Cenomanian micromorphic ammonites from the western interior of the USA: Palaeontology, v. 33, p. 379–422.
- 963 KENNEDY, W.J., and KLINGER, H.C., 1975, Cretaceous faunas from Zululand and Natal, South Africa.
- Introduction, stratigraphy: Bulletin of the British Museum (Natural History), Geology, v. 25, p. 263–
- 965 315.

957

- 966 KENNEDY, W.J., COBBAN, W.A., HANCOCK, J.M., and GALE, A.S., 2005, Upper Albian and Lower
- Cenomanian ammonites from the Main Street Limestone, Grayson Marl, and Del Rio Clay in northeast
- Texas: Cretaceous Research, v. 26, p. 349–428.
- KEUPP, H., 2012, Atlas zur paläopathologie der cephalopodan: Berliner Paläobiologische Abhandlungen, v.
- 970 12, p. 1–392.
- 971 KLINGER, H.C., 1981, Speculations on buoyancy control and ecology in some heteromorph ammonites, in
- House, M.R., and Senior, J.R. (eds.), The Ammonoidea: Systematics Association Special Volume No.
- 973 18. Systematic Association, London, p. 337–355.
- 974 KLINGER, H.C., and KENNEDY, W.J., 1978, Turrilitidae (Cretaceous Ammonoidea) from South Africa, with
- a discussion of the evolution and limits of the family: Journal of Molluscan Studies, v. 44, p. 1-48.
- 976 KLUG, C. and LEHMANN, J., 2015, Soft part anatomy of ammonoids: reconstructing the animal based on
- exceptionally preserved specimens and actualistic comparisons. in Klug, C., Korn, D., De Baets, K.,
- Kruta, I., and Mapes, R.H. (eds.), Ammonoid paleobiology. Vol. 1: from anatomy to ecology: Topics in
- Geobiology, 43. Springer, Dordrecht, The Netherlands, p. 515–538.
- 980 KLUG, C., RIEGRAF, W. and LEHMANN, J., 2012, Soft-part preservation in heteromorph ammonites from
- the Cenomanian-Turonian Boundary Even (OAE 2) in the Teutoburger Wald (Germany): Palaeontology,
- 982 v. 55, p. 1307–1331.
- 983 KLUG, C., KRÖGER, K., VINTHER, J., FUCHS, D., and DE BAETS, K., 2015, Ancestry, origin and early
- evolution of ammonoids, *in* Klug, C., Korn, D., De Baets, K., Kruta, I., and Mapes, R.H. (eds.),
- Ammonoid paleobiology, from macroevolution to paleogeography: Topics in Geobiology, 44. Springer,
- Dordrecht, The Netherlands, p. 3–24.
- 987 KRÖGER, B., VINTHER, J., and FUCHS, D., 2011, Cephalopod origin and evolution: A congruent picture
- emerging from fossils, development and molecules: Bioessays, v. 33, p. 602–613.

- 989 KRUTA, I., LANDMAN, N., TANABE, K., and CECCA, F., 2009, Aptychus microstructure in Late
- 990 Cretaceous Ancyloceratina (Ammonoidea): Lethaia, v. 42, p. 312–321.
- 991 KRUTA, I., LANDMAN, N., ROUGET, I., CECCA, F., and LARSON, N., 2010, The jaw apparatus of the Late
- Cretaceous ammonite *Didymoceras*: Journal of Paleontology, v. 84, p. 556–560.
- 993 KRUTA, I., LANDMAN, N., ROUGET, I., CECCA, F., and TAFFOREAU, P., 2011, The role of ammonites in
- the Mesozoic marine food web revealed by jaw preservation: Science, v. 331, p. 70–72.
- 995 KURIHARA, K., TOSHIMITSU, S., and HIRANO, H., 2012, Ammonoid biodiversity changes across the
- Cenomanian-Turonian boundary in the Yezo Group, Hokkaido, Japan: Acta Palaeontologica Polonica,
- 997 v. 57, p. 749–757.
- 998 LAMARCK, J.B.P.A. DE M. DE, 1801, Systéme des Animaux sans vertébrés, Deterville, Paris, 432 p.
- LANDMAN, N.H., TANABE, K., and SHIGETA, Y., 1996, Ammonoid embryonic development, in Landman,
- N.H., Tanabe, K., and Davis, R.A., (eds.), Ammonoid Paleobiology, Plenum Press, New York, p. 344–
- 001 399.
- LECKIE, R.M., BRALOWER, T.J., and CASHMAN, R., 2002, Oceanic anoxia events and plankton evolution:
- biotic response to tectonic forcing during the mid-Cretaceous: Paleoceanography, v. 17, p. PA623.
- 004 LEMANIS, R., ZACHOW, S., FUSSEIS, F., HOFFMANN, R., 2015, A new approach using high-resolution
- computed tomography to test the buoyant properties of chambered cephalopod shells: Paleobiology, v.
- 006 41, p. 313–329.
- 007 LUKENEDER, A., HARZHAUSER, M., MUELLEGGER, S., and PILLER, W.E., 2010, Ontogeny and habitat
- change in Mesozoic cephalopods revealed by stable isotopes (δ^{18} O, δ^{13} C): Earth and Planetary Science
- 009 Letters, v. 296, p. 103–114.
- 010 MATSUMOTO, T., INOMA, A., and KAWASHITA, Y., 1999, The turrilitid ammonoid *Mariella* from
- Hokkaido Part 1 (Studies of the Cretaceous ammonites from Hokkaido and Sakhalin–LXXXV):
- Paleontological Research, v. 3, p. 106–120.

MATSUMOTO, T., and KAWASHITA, Y., 1999, The turrilitid ammonoid *Mariella* from Hokkaido – Part 2 (Studies of the Cretaceous ammonites from Hokkaido and Sakhalin–LXXXVI): Paleontological Research, v. 3, p. 162–172.

- MONNET, C., 2009, The Cenomanian–Turonian boundary mass extinction (Late Cretaceous): new insights from ammonoid biodiversity patterns of Europe, Tunisia and the Western Interior (North America): Palaeogeography, Palaeoclimatology, Palaeoecology, v. 282, p. 88–104.
- MONNET, C., and BUCHER, H., 2007, European ammonoid diversity questions the spreading of anoxia as primary cause for the Cenomanian/Turonian (Late Cretaceous) mass extinction: Swiss Journal of Geosciences, v. 100, p. 137–144, doi:10.1007/s00015-007-1209-1.
- MONNET, C., BUCHER, H., ESCARGUEL, G., and GUEX, J., 2003, Cenomanian (early Late Cretaceous) ammonoid faunas of Western Europe. Part II: diversity patterns and the end-Cenomanian anoxic event. Eclogae Geologicae Helvetiae, v. 96, p. 381–398.
- MONNET, C. KLUG, C., and De Baets, K., 2015, Evolutionary patterns of ammonoids: phenotypic trends, convergence, and parallel evolution, *in* Klug, C., Korn, D., De Baets, K., Kruta, I., and Mapes, R.H. (eds.), Ammonoid paleobiology. from macroevolution to paleogeography: Topics in Geobiology, 44. Springer, Dordrecht, The Netherlands, p. 95–142.
- MONTEIRO, F.M., PANCOST, R.D., RIDGWELL, A., DONNADIEU, Y., 2012, Nutrients as the dominant control on the spread of anoxia and euxinia across the Cenomanian–Turonian oceanic anoxic event (OAE2): model-data comparison: Paleoceanography, v. 27, p. PA4209.
- NAGLIK, C., TAJIKA, A., CHAMBERLAIN, J., and KLUG, C., 2015a, Ammonoid locomotion, *in* Klug, C., Korn, D., De Baets, K., Kruta, I., and Mapes, R.H. (eds.), Ammonoid paleobiology. from anatomy to ecology: Topics in Geobiology, 43. Springer, Dordrecht, The Netherlands, p. 649–688.

- NAGLIK, C., MONNET, C., GOETZ, S., KOLB, C., DE BAETS, K., TAJIKA, A., and KLUG, C., 2015b,
- O36 Growth trajectories of some major ammonoid sub-clades revealed by serial grinding tomography data:
- 037 Lethaia, v. 48, p. 29–46.
- NAGLIK, C., RIKHTEGAR, F., and KLUG, C., 2016, Buoyancy of some Palaeozoic ammonoids and their
- hydrostatic properties based on empirical 3D-models: Lethaia, v. 49, p. 3–12.
- OKAMOTO, T., 1996, Theoretical modeling of ammonoid morphology, in Landman, N.H., Tanabe, K., and
- Davis, R.A., (eds.), Ammonoid Paleobiology, Plenum Press, New York. p. 225–251.
- OLDE, K., JARVIS, I., ULICNY, D., PEARCE, M.A., TRABUCHO-ALEXANDRE, J.T., CECH, S.,
 - GROCKE, D.R., LAURIN, J., SVABENICKA, L., and TOCHER, B.A., 2015, Geochemical and
 - palynological sea-level proxies in hemipelagic sediments: A critical assessment from the Upper
 - Cretaceous of the Czech Republic: Palaeogeography, Palaeoclimatology, and Palaeoecology, v. 435, p.
- 046 222–243.

044

045

048

- PAGE, K.N., 1996, Mesozoic ammonoids in space and time, in Landman, N., Tanabe, K., and Davis, R.A.
 - (eds.), Ammonoid paleobiology. Topics in geobiology 13, Plenum, New York, USA, p. 755–794.
- PETERMAN, D.J., and BARTON, C.C., 2019, Power scaling of ammonitic suture patterns from Cretaceous
 - Ancyloceratina: constraints on septal/sutural complexity: Lethaia, v. 52, p. 77–90.
- PETERMAN, D.J., CIAMPAGLIO, C.N., SHELL, R.C. and YACOBUCCI, M.M., 2019, Mode of life and
- hydrostatic stability of orthoconic ectocochleate cephalopods: hydrodynamic analyses of restoring
- moments from 3D-printed, neutrally buoyant modes of a baculite: Acta Palaeontologica Polonica, v. 64,
- p. 441–460, doi:10.4202/app.00595.2019.
- 055 PETERMAN, D.J., YACOBUCCI, M.M., LARSON, N.L., CIAMPAGLIO, C.N. and LINN, T., 2020a, A
- method to the madness: ontogenetic changes in the hydrostatic properties of *Didymoceras*
- 057 (Nostoceratidae, Ammonoidea): Paleobiology, v. 46, p. 237–258, doi:10.1017/pab.2020.14.

- 058 PETERMAN, D.J., HEBDON, N., CIAMPAGLIO, C.N., YACOBUCCI, M.M., LANDMAN, N.H. and LINN,
- T., 2020b, Syn vivo hydrostatic and hydrodynamic properties of scaphitid ammonoids from the U.S.
- 060 Western Interior: Geobios, v. 60, p. 79–98, doi: 10.1016/j.geobios.2020.04.004.
- PETERMAN, D.J., SHELL, R.C., CIAMPAGLIO, C.C., and YACOBUCCI, M.M., 2020c, Stable hooks:
- biomechanics of heteromorph ammonoids with U-shaped body chambers: Journal of Molluscan Studies,
- v. 86, p. 267–279, doi:10.1093/mollus/eyaa018.
- PETERMAN, D.J., MIKAMI, T., and INOUE, S., 2020d, The balancing act of *Nipponites mirabilis*
- 065 (Nostoceratidae, Ammonoidea): Managing hydrostatics throughout a complex ontogeny: PLOS ONE, v.
- 066 15, p. 1–23, doi:10.1371/journal.pone.0235180.
- POULSEN, C.J., TABOR, C., and WHITE, J.D., 2015, Long-term climate forcing by atmospheric oxygen
- oncentrations: Science, v. 348, p. 1238–1241.
- 069 RAUP, D.M., and SEPKOSKI, J.J., 1986, Periodic extinction of families and genera: Science, v. 231, p. 833–
- 070 836.
- 071 RITTERBUSH, K.A., HOFFMANN, R., LUKENEDER, A., and DE BAETS, K., 2014, Pelagic palaeoecology:
- the importance of recent constraints on ammonoid palaeobiology and life history: Journal of Zoology, v.
- 073 292, p. 229–241.
- 074 ROEMER, F.A., 1852, Die Kreidebildungen von Texas und ihre organischen Einschlüsse. Adolph Marcus,
- 075 Bonn, 100 pp.
- 076 TAJIKA, A., NAGLIK, C., MORIMOTO, N., PASCUAL-CEBRIAN, E., HENNHÖFER, D.K., and KLUG,
- 077 C., 2015, Empirical 3D-model of the conch of the Middle Jurassic ammonite microconch *Normannites*,
- ors its buoyancy, the physical effects of its mature modifications and speculations on their function:
- 079 Historical Biology, v. 27, p. 181–191.
- 080 TEICHERT, C., KUMMEL, B., SWEET, W.C., STENZEL, H.B., FURNISH, W.M., GLENISTER, B.F.,
- ERBEN, H.K., MOORE, R.C., and ZELLER, D.E., 1964, Treatise on Invertebrate Paleontology, Part K,

- Mollusca 3, Cephalopoda General Features, Endoceratoidea, Actinoceratoidea, Nautiloidea,
- Bactritoidea. Universeity of Kansas Press, Lawrence, KS, USA.
- TRUEMAN, A.E., The ammonite body chamber, with special reference to the buoyancy and mode of life of the
- living ammonite: Quarterly Journal of the Geological Society of London, v. 1941, p. 339–383.
- 086 WARD, P.D., 1979a, Functional morphology of Cretaceous helically-coiled ammonite shells: Paleobiology, v.
- 087 5, p. 415–422.

- WARD, P.D., 1979b, Cameral liquid in *Nautilus* and ammonites: Paleobiology, v. 5, p. 40–49.
- 089 WARD, P.D., and MARTIN, A., 1978, On the buoyancy of the Pearly *Nautilus*: A Willey's zoological results:
- O90 Cambridge University Press, London, v. 6, p. 691–830.
- 091 WEITSCHAT, W., and BANDEL, K., 1991, Organic components in phragmocones of boreal Triassic
- ammonoids: implications for ammonoid biology: Paläontologische Zeitschrift, v. 65, p. 269–303.
- WELLS, M.J., and O'DOR, R.K., 1991, Jet propulsion and the evolution of the cephalopods: Bulletin of Marine
- 094 Science, v. 49, p. 419–432.
- 095 WESTERMANN, G.E.G. 1996. Ammonoid life and habitat, in Landman, N.H., Tanabe, K., and Davis, R.A.,
- 096 (eds.), Ammonoid Paleobiology, Plenum Press, New York. p. 607–707.
- 097 WIEDMANN, J., 1973, Upper Triassic heteromorph ammonites, in Hallam A. (ed.), Atlas of
- Paleobiogeography: Elsevier, Amsterdam, p. 235–244.
- 099 WRIGHT, C.W., CALLOMAN, J.H., and HOWARTH, M.K., 1996, Treatise on invertebrate paleontology. Part
- L, revised: Mollusca 4 (Cretaceous Ammonoidea). University of Kansas Press, Lawrence, KS, USA.
- 101 YACOBUCCI, M.M., 2017, Marine life in a greenhouse world: cephalopod biodiversity and biogeography
- during the early Late Cretaceous: Paleobiology, v. 43, p. 587–619, doi:10.1017/pab.2017.3.
- 2103 ZHENG, X., JENKYNS, H.C., GALE, A.S., WARD, D.J., and HENDERSON, G.M., 2016, A climatic control
- on reorganization of ocean circulation during the mid-Cenomanian event and Cenomanian-Turonian
- oceanic anoxic event (OAE 2): Nd isotope evidence: Geology, v. 44, p. 151–154.

107

108

109

110

111

112

113

114

115

116

117

118

119

120

121

122

123

124

125

126

127

128

129

130

131

132

FIGURE CAPTIONS

Figure 1: Hydrostatic measurements of torticones, A) Side view in life orientation showing the measurement of the apertural angle (θ_a), and thrust angle (θ_t). B) Vertical view, depicting the measurement of the rotational thrust angle (θ_{tr}). C) Front view, denoting the lever arm (L_x) that produces torque during jet propulsion. B = center of buoyancy, M = center of mass, R = horizontal rotation pivot point, H = hyponome, source of jet thrust. Figure 2: Construction of a 3D printed torticone model for physical experimentation. A) Virtual hydrostatic model with complex internal geometry and nonuniform density which govern the mass distribution. The points of the upper cone and lower cone correspond to the centers of buoyancy and mass, respectively. B) Virtual model simplified for printing, while maintaining the mass distribution of the complex hydrostatic model. An air filled void and steel wire counterweight correct for the differences in mass and its distribution, and allow the model to be 3D printed in uniform density PLA (polylactic acid) filament. C) 3D Printed torticone model. D) Top view showing the location of the tracking points used to determine angular displacement, angular velocity, and angular acceleration. Figure 3: Final hydrostatic models of *Mariella brazoensis* oriented according to their life position. A) Side view. B) Vertical view showing the ideal direction of thrust for pure rotation. C) Front view. The points of the upper and lower cones correspond to the centers of buoyancy and mass, respectively. R = pivot point for rotation about some horizontal axis, H = location of hyponome, source of jet thrust, Dashed line = vertical rotation axis. **Figure 4:** Smoothed version of the hydrostatic model of *Mariella brazoensis*. The points of the upper and lower cones correspond to the centers of buoyancy and mass, respectively. Figure 5: Results of computational fluid dynamics (CFD) simulations showing streamlines passing over the torticone model. A) Torticone moving in the upward direction at 10 cm/s, B) Enlarged view drawing attention to rotating streamlines. Arrows denote the relative flow direction of the fluid. Figure 6: Results of computational fluid dynamics (CFD) simulations showing streamlines passing over the torticone model. A) Torticone moving in the downward direction at 10 cm/s. B) Enlarged view showing pressure contours along the underside of the shell. Arrows denote the relative flow direction of the fluid. Figure 7: Computational fluid dynamics simulations showing cross sections of the models and the surrounding fluid

velocity within this plane. Arrows denote movement direction of the torticone. A) Upward movement. B) Downward

movement. C) Horizontal movement (aperture-backwards direction). Movement in the vertical directions is more streamlined, while the horizontal direction produces more hydrodynamic drag.

Figure 8: Motion tracking results of the vertical motion experiments on the ornamented and smooth physical models. A) Angular displacement (in degrees) from the starting position and B) angular velocities (degrees/s) for models with *Nautilus*-like thrusts. B) Angular displacement (in degrees) from the starting position and D) angular velocities (degrees/s) for models with coleoid-like thrusts. Positive values denote aperture-backwards rotation, which occurred during upward movement. Negative values denote aperture-forwards rotation, which occurred during downward movement.

Figure 9: Motion tracking results of the neutrally buoyant *Mariella brazoensis* model. A) Angular velocities of 15 trials where the model was pushed at differing initial angular velocities. Afterwards hydrodynamic drag was responsible for decelerating the model. B) Torques occurring on the model in response to interaction with the surrounding fluid. C) Close up of torque values with dashed line representing the torques produced at the hyponome during ventilation of the gills (13.2 dyn·cm). D) Close up of angular velocities. Light green points correspond to thrusts produced by ventilation of the gills, suggesting that angular velocities of around 17 to 22 degrees per second could be sustained with this metabolically inexpensive process.

Figure 10: Depiction of movement directions during physical experiments. A) Upward movement resulting in consistent aperture-backwards rotation. B) Downward movement resulting in consistent aperture-forwards rotation. C) Depiction of the precession of the shell's coiling axis (dashed line showing path) about the vertical axis (black point in center).

TABLE CAPTIONS

Table 1: Array instructions used to build the shell of *Mariella brazoensis*. Large, arbitrary initial dimensions were used to avoid round-off error. The initial whorl section size, with a particular center, was translated, rotated, and scaled in the x, y, and z directions to build the shell from the aperture to the apex. The center of the initial whorl section serves as the datum for these transformations. Shell ornamentation and septa were also replicated with these instructions.

Table 2: Hydrostatic properties of the ornamented and smooth *Mariella brazoensis* models. Φ = conditions for neutral buoyancy (i.e., the percentage of the phragmocone to be emptied of cameral liquid). S_t = hydrostatic stability index. θ_a = apertural angle. θ_t = thrust angle. θ_{tr} = rotational thrust angle. Measurements further defined in Figure 1.

Table 3: Hydrodynamic drag forces computed during computational fluid dynamics simulations in the upward, downward, and horizontal directions of movement. The x, y, and z components of drag force are reported from two velocities within the range of the physical experiments. Bold numbers refer to drag forces occurring in the direction of movement.

Table 4: Error in thrust values for each physical experiment (which are simulated by buoyancy surpluses or deficiencies). Such errors are a result of mass differences in in the PLA models and their counterweights, causing deviation from the target buoyancy values.

Table 5: Initial angular velocities (ω; degrees per second) for each trial of the neutrally buoyant rotation experiment. R² values and coefficients are reported for the regression lines of angular displacement in the form: (a*t)/(1+b*t). These equations for each trial were later differentiated to compute angular velocity and angular acceleration.